Journal of Process Control 116 (2022) 34–52

Contents lists available at ScienceDirect

Journal of Process Control

journal homepage: www.elsevier.com/locate/jprocont

Approaches based on LAMDA control applied to regulate HVAC systems for buildings

L. Morales [a], D. Pozo-Espín [b], J. Aguilar [c,d,e,*], M.D. R-Moreno [e,f]

[a] Departamento de Automatización y Control Industrial, Escuela Politécnica Nacional, Quito, Ecuador
[b] Ingeniería y Ciencias Aplicadas, Universidad de Las Américas, Quito, Ecuador
[c] CEMISID, Facultad de Ingeniería, Universidad de Los Andes, Mérida 5101, Venezuela
[d] GIDITIC, Universidad EAFIT, Medellín, Colombia
[e] Universidad de Alcalá, Dpto. de Automática, Alcalá de Henares, Spain
[f] TNO, Intelligent Autonomous Systems Group (IAS), The Hague, The Netherlands

ARTICLE INFO

Article history:
Received 16 January 2022
Received in revised form 13 April 2022
Accepted 27 May 2022
Available online 11 June 2022

Keywords:
LAMDA
SMC
Intelligent control
Nonlinear systems
HVAC systems

ABSTRACT

The control of HVAC (Heating Ventilation and Air Conditioning) systems is usually complex because its modeling in certain cases is difficult, since these systems have a large number of components. Heat exchangers, chillers, valves, sensors, and actuators, increase the non-linear characteristics of the complete model, so it is necessary to propose new control strategies that can handle the uncertainty generated by all these elements working together. On the other hand, artificial intelligence is a powerful tool that allows improving the performance of control systems with inexact models and uncertainties. This paper presents new control alternatives for HVAC systems based on LAMDA (Learning Algorithm for Multivariable Data Analysis). This algorithm has been used in the field of machine learning, however, we have taken advantage of its learning characteristics to propose different types of intelligent controllers to improve the performance of the overall control system in tasks of regulation and reference change. In order to perform a comparative analysis in the context of HVAC systems, conventional methods such as PID and Fuzzy-PID are compared with LAMDA-PID, LAMDA-Sliding Mode Control based on Z-numbers (ZLSMC), and Adaptive LAMDA. Specifically, two HVAC systems are implemented by simulations to evaluate the proposals: an MIMO (Multiple-input Multiple-output) HVAC system and an HVAC system with dead time, which are used to compare the results qualitatively and quantitatively. The results show that ZLSMC is the most robust controller, which efficiently controls HVAC systems in cases of reference changes and the presence of disturbances.

1. Introduction

Heating, Ventilation, and Air-Conditioning (HVAC) systems are a key point in buildings energy consumption, being its correct design a fundamental part of energy-saving policies. The growth of the commercial and residential sectors brings with it high energy consumption, reaching 40% of the total energy used in the world, much of which (between 40%–70%) is used by HVAC systems [1]. Likewise, if energy consumption is considered only at the residential level, then this reaches 25%, of which 64% is allocated to HVAC systems [2]. Moreover, one of the main challenges in the HVAC systems design for buildings is to generate the necessary comfort conditions for people inside their homes or workplaces, while maintaining low energy consumption through adequate control of the systems [3,4].

In this context, several works have approached the subject from different points of view, focusing on: modeling of systems [5–7], traditional control methods [8–12], Fuzzy control [2,13–15], Predictive–Adaptive control [16–18], Sliding mode control [19], stochastic optimal control [20], modeling and fault detection [21–23], modeling and control methods based on Machine Learning (ML) [24,25] and Deep Learning (DL) [26,27], among others.

System modeling and simulation are essential for the understanding and development of control methods for HVAC systems. In works like [28], comparisons between different controllers are performed, while in [29] is carefully reviewed the different types of modeling, depending on their application, their main characteristics, shortcomings and outcomes. Moreover, [30,31] proposed simulation tools to analyze the different components and their behaviors in HVAC systems.

* Corresponding author at: Universidad de Alcalá, Dpto. de Automática, Alcalá de Henares, Spain.
E-mail addresses: luis.moralesec@epn.edu.ec (L. Morales), david.pozo@udla.edu.ec (D. Pozo-Espín), aguilar@ula.ve, aguilarjos@gmail.com (J. Aguilar), malola.rmoreno@uah.es (M.D. R-Moreno).

https://doi.org/10.1016/j.jprocont.2022.05.013

Although there are several studies on HVAC modeling in different environments of use, as well as traditional control systems for its correct operation, these can become extremely complex. In this way, works like [32] point to the use of techniques based on DL that allow obtaining a reliable, robust and scalable system despite the non-linearities and uncertainties of the system, such as: dead time, physical characteristics of the work environment, occupants, and external temperature, among others.

Artificial Intelligence (AI) techniques can improve the performance of HVAC systems due to their machine learning features, which can help manage uncertainty, as presented in [33]. One of these techniques is LAMDA (Learning Algorithm for Multivariable Data Analysis), a method initially proposed for clustering and classification tasks, which has recently been used to work in the field of control systems. The main characteristics of LAMDA are:

- LAMDA can work as a classification (supervised learning) and clustering (unsupervised learning) algorithm (purpose for which the algorithm was created).
- LAMDA is not computationally expensive.
- LAMDA has a fixed and known number of layers where all the coefficients can be customized by the user.
- LAMDA has no complex mathematical operations.

The advantages of LAMDA have motivated us to work with this algorithm in the field of process control, proposing new schemes with particular characteristics for each of them. Initially, in [34] has been proposed an inference stage that allows the system to be controlled to the desired state of zero error. This controller has been called LAMDA-PID (Proportional-Integral-Derivative), which has presented promising results in terms of performance. In [35] has been defined an Adaptive LAMDA for fuzzy control and modeling of systems, modifying the LAMDA structure with the addition of layers that operate similarly to Artificial Neural Networks, but with the advantage of having a fixed number of layers whose calibration is not trivial. Adaptive LAMDA is computationally more expensive than the original LAMDA controller; however, it is adequate in applications with complex, unknown or variable dynamics. The paper [36] formalizes a LAMDA algorithm for control based on the fundamentals of the Lyapunov theory and the Sliding-Mode Control (SMC), in order to guarantee stability and robustness, respectively. This proposal is called LAMDA–SMC (LSMC), and combines the features of LAMDA with those of the SMC to obtain a chattering-free control output. Finally, in [37] is proposed a methodology to improve the performance of LSMC by combining it with the concepts of Z-numbers since this last theory allows handling the uncertainty through the principle of reliability. The proposal is called ZLSMC [38], and allows control systems with uncertainties with excellent results.

The main contribution of this work is the design of LAMDA-based fuzzy control models for HVAC systems. In particular, the article describes the formulation of control models for different HVAC systems existing in the literature, and makes an in-depth analysis of their behavior in various operating scenarios to show their versatility and robustness. Thus, based on the different characteristics of the recent LAMDA controllers as learning, robustness and disturbance rejection, the novelty of this paper is the application of the different proposals of LAMDA in the regulation of HVAC systems for buildings (systems very different from those that have been used to validate these proposals). The HVAC systems are complex to model due to the variety and quantity of elements that interact in the system such as: heat exchangers, chillers, valves, sensors, and actuators, which increase the non-linear characteristics of the system model. LAMDA is capable of regulating systems with modeling uncertainty, as seen in the previously cited works, in which our controllers have excellent responses in terms of disturbance rejection. Likewise, we have been able to verify through exhaustive experimentation that LAMDA presents an excellent performance in regulation and tracking reference. Thus, we consider that this work is an important contribution in the context of the control of HVAC systems. The remainder of the paper is structured as follows: Section 2 describes the fundamentals of the different proposals of LAMDA in the field of process control. Section 3 details the models of the HVAC systems used to validate the LAMDA controllers. Simulations and a deep analysis of the results are presented in Section 4. Finally, the conclusions of the paper are discussed.

2. LAMDA control approaches

This subsection presents a brief description of the different controller proposals based on LAMDA, in order to establish the basis for the reader's understanding of the operation and design of the different approaches.

2.1. LAMDA control

LAMDA is a method of AI used to categorize functional states of systems. The algorithm does a similitude exploration among the descriptors of one individual $O = [o_1; \ldots; o_j; \ldots; o_l]$ and the existing classes/clusters $C = \{C_1; \ldots; C_k; \ldots; C_m\}$, to calculate its membership degree [39]. Initially, LAMDA normalizes the descriptors of the individual O in a range between [0.1], in order to place all of them in the same subspace. The normalized descriptor $\bar{o}_j$ is calculated as:

$$\bar{o}_j = \frac{o_j - o_{jmin}}{o_{jmax} - o_{jmin}} \tag{1}$$

Where:
o_{jmax}: the maximum value of the descriptor o_j
o_{jmin}: the minimum value of the descriptor o_j

2.1.1. Marginal adequacy degree (MAD)

The MADs compute the similarity between the descriptor of the object with the corresponding descriptor in each class. Probability density functions, like the Gaussian, are used to calculate the MADs. This function requires the average of the descriptor j in the class k ($\rho_{k,j}$) and its standard deviation $\sigma_{k,j}$ [37], which are computed as:

$$MAD_{k,j} = e^{-\frac{1}{2}\left(\frac{\bar{o}_j - \rho_{k,j}}{\sigma_{k,j}}\right)^2} \tag{2}$$

$$\rho_{k,j} = \frac{1}{n_{k,j}} \sum_{t=1}^{n_{k,j}} \bar{o}_j(t) \tag{3}$$

$$\sigma_{k,j}{}^2 = \frac{1}{n_{k,j} - 1} \sum_{t=1}^{n_{k,j}} (\bar{o}_j(t) - \rho_{k,j})^2 \tag{4}$$

Where:
$n_{k,j}$: number of elements of the descriptor j in the class k.
$\rho_{k,j}$ and $\sigma_{k,j}$: values computed in the training stage based on the elements of each class.

2.1.2. Global adequacy degree (GAD)

The GADs are values calculated by mixing the MADs with fuzzy logic operators as the Dombi operator. The GADs compute the membership degree of one individual in each class. The Dombi operator is composed of the T-norm "$T(a, b)$" and the S-norm "$S(a, b)$" defined as:

$$\begin{aligned} T(a, b) &= \frac{1}{1 + \sqrt[p]{\left(\frac{1-a}{a}\right)^p + \left(\frac{1-b}{b}\right)^p}}; \\ S(a, b) &= 1 - \frac{1}{1 + \sqrt[p]{\left(\frac{a}{1-a}\right)^p + \left(\frac{b}{1-b}\right)^p}} \end{aligned} \tag{5}$$

The values a, b are the MADs in the class k, and $p \geq 1$ modifies the sensitivity of the function. The GAD of the individual $\bar{O}$, defined as $\bar{O} = [\bar{o_1}; \ldots; \bar{o_j}; \ldots; \bar{o_l}]$, in the class k is obtained as:

$$GAD_{k,\bar{O}}\left(MAD_{k,1}, \ldots, MAD_{k,l}\right) = \alpha T\left(MAD_{k,1}, \ldots, MAD_{k,l}\right) + (1-\alpha)\, S\left(MAD_{k,1}, \ldots, MAD_{k,l}\right) \tag{6}$$

where $0 \leq \alpha \leq 1$ is the exigency coefficient. If α decreases, then the LAMDA algorithm is permissive; and if α increases, then the algorithm is stricter [40].

In control systems, an individual is defined by the GADs. Thus, LAMDA must identify the current state of the system and, in order to take it to the desired one [33]. In the paper [36] has been proposed an inference method to establish a LAMDA controller. For this purpose, it is required to define classes and rules as in conventional fuzzy controllers. In our approach, it is important to understand how LAMDA works based on rules (see Eq. (7)). Thus, the expression that summarizes the fuzzy inference mechanism for LAMDA based on rules is:

$$R^{(k)}: IFo_1 \text{ is } F_1^p \text{ and } \ldots o_j \text{ is } F_j^q \ldots \text{ and } o_l \text{ is } F_l^r \text{ THEN } y_k \text{ is } G_k \tag{7}$$

where o_j is the object descriptor taking values in the universe of discourse U_j. y_k takes values of the universe of discourse V. The fuzzy set $F_j = \left\{F_j^q : q = 1, 2, \ldots, Q\right\}$ belongs to U_j, the fuzzy set G_k belongs to V, and $Rule^{(k)}$ is the rule applied to the class k.

The LAMDA inference mechanism uses the GADs of each class and the first order Takagi–Sugeno Kang (TSK) inference method [41], where γ_k is a weight applied to each class (singleton function). To calculate the controller output, the following expression is proposed:

$$u = \left| \frac{\arg\max\left(\gamma_k\right)}{\sum_{k=1}^{m} \gamma_k GAD_{k,\text{argmax}(\bar{o})}} \right| \sum_{k=1}^{m} \gamma_k GAD_{k,\bar{O}} \tag{8}$$

where u is the output of the controller. The term calculated in the absolute value corresponds to a coefficient that limits the calculation of the control output u to values between $[-1\ 1]$ when the descriptors are at the limit of the universe of discourse.

2.2. LAMDA sliding-mode control based on Z-numbers (ZLSMC)

The ZLSMC is an enhancement of the proposed LAMDA–SMC (LSMC) [36,38]. Considering that most processes can be simplified to second or third order, ZLSMC is designed assuming a system modeled in a canonical form as:

$$\begin{aligned} &\dot{x}_i(t) = x_{i+1}(t), \quad 1 \leq i \leq n-1 \\ &\dot{x}_n(t) = A\left(X,t\right) + b\left(X,t\right) u(t) + d(t) \end{aligned} \tag{9}$$

where: $X(t) = [x_1(t), x_2(t), \ldots, x_n(t)]^T = \left[x(t), \dot{x}(t), \ldots, x^{(n-1)}(t)\right]^T \epsilon \Re^n$ is the state vector of the system, $A\left(X,t\right)$ and $b\left(X,t\right)$ are inexact (partially known) continuous nonlinear bounded functions, $u(t) \in \Re$ is the control input, $d(t) \in \Re$ is the external bounded disturbance, $b\left(X,t\right)$ is an upper and lower bounded function defined as $0 < b < |b\left(X,t\right)| < \bar{b}$. $A\left(X,t\right)$, thus:

$$|A\left(X,t\right)| \leq \beta_A \text{ and } |d(t)| \leq \beta_d \tag{10}$$

where β_A, β_d are positive.

The control goal of ZLSMC is to compute a control action for the system to track an n-dimensional desired state $X_d(t) = [x_{d1}(t), x_{d2}(t), \ldots, x_{dn}(t)]^T =, \left[x_d(t), \dot{x}_d(t), \ldots, x_d^{(n-1)}(t)\right]^T$, considering an inaccurate model and disturbances. Thus, the error is defined as:

$$E(t) = X_d(t) - X(t) = \left[e(t), \dot{e}(t), \ldots, e^{(n-1)}(t)\right]^T \tag{11}$$

For any desired trajectory $X_d(t)$, the tracking error vector must satisfy the Euclidean norm:

$$\lim_{t\to\infty} \|E(t)\| = \lim_{t\to\infty} \|X_d(t) - X(t)\| \to 0 \tag{12}$$

For the ZSMC, it is required to define a continuous sliding surface where the system can slide to the desired state. The sliding surface for a system of $n-$ order is defined as [42]:

$$s(t) = \left(\frac{d}{dt} + \lambda\right)^n \int e(t)dt \tag{13}$$

In the ZLSMC, LAMDA is used to obtain the continuous and discontinuous control actions u_c and u_d, respectively. u_d is the control action used on the sliding surface, and u_c is the control action to maintain the system on the sliding surface. Thus, the complete control action of the controller is $u = u_c + u_d$.

Developing (13):

$$s(t) = \frac{d^{n-1}e(t)}{dt} + r_{n-1}\lambda \frac{d^{n-2}e(t)}{dt} + r_{n-2}\lambda^2 \frac{d^{n-3}e(t)}{dt} + \cdots + \lambda^n \int e(t)dt \tag{14}$$

with $r_0 = 1$ and $e^{(0)}(t) = e(t)$.

From (12), the n-derivative of the error $e^{(n)}(t)$ is computed as:

$$e^{(n)}(t) = \dot{x}_{dn}(t) - \dot{x}_n(t) \tag{15}$$

$$e^{(n)}(t) = \dot{x}_{dn}(t) - A\left(X,t\right) - b\left(X,t\right) u - d(t) \tag{16}$$

If $u = u_c$ for the continuous control law, replacing (16) in the first derivative of (14), we have:

$$\dot{s}(t) = \dot{x}_{dn}(t) - A\left(X,t\right) - b\left(X,t\right) u_c - d(t) + \sum_{i=1}^{n} r_{n-i}\lambda^i e^{(n-i)} \tag{17}$$

To obtain $\dot{s}(t) = 0$, based on (18) it is required to identify the sign of the function $b\left(X,t\right)$ to set the rules for the classes. If $b\left(X,t\right) > 0$, then $\dot{s}(t)$ decreases as u_c increases and vice versa. This information is used to define a set of rules based on the LAMDA classes to obtain $\dot{s}(t) = 0$. In this paper, are used five classes for $\dot{s}(t)$, as detailed in [36]. The fuzzy sets for the classes of the variable $\dot{s}(t)$ are Negative Big ($NB = -1$), Negative Small ($NS = -0.5$), zero ($ZE = 0$), Positive Small ($PS = 0.5$), and Positive Big ($PB = 1$). These classes are used to compute the normalized continuous control action u_{nc}. For calibration, the scaling gain k_1 is used at the input $\dot{s}(t)$, and the scaling gain k_c at the output as:

$$u_c = k_c u_{nc} \quad \Longrightarrow \quad u_c = k_c ZLSMC\left(\dot{s}\right); \quad k_c > 0 \tag{18}$$

The rule table of the continuous control action is presented in Table 1, considering $C_k = (\gamma_k, R_c)$; $\forall k = \{1, 2, \ldots, 5\}$.

Table 1 shows that the classes per descriptor and the membership functions of the reliability are required. Note that for the reliability part, the absolute value of $\dot{s}$ is used (see Fig. 1). Abiyev and Akkaya [43] proposed three classes to represent reliability in a simple and complete way for control systems, these are: "S" is "sometimes", "U" is "usually", and "A" is "always".

There are two descriptors as LAMDA inputs; therefore, (2) is computed for s and its derivative, that is $j = 1$ for $\dot{s}$ and $j = 2$ for s. The calculation of the new class centers is made based on the Total Utility of Z-numbers $TU(Z)$ proposed in [44]. $TU_{k,j}(Z)$ is applied to the descriptor $\dot{s}$ as:

$$TU_{k,1}(Z) = TU\left(MAD_{k,1}, R_1\right) = \frac{\rho_{k,1} c_{R_1}}{\left(1 + 8{\sigma_{k,1}}^2\right)\left(1 + 8{\sigma_{R_1}}^2\right)} \tag{19}$$

where $R_1 = Gauss(c_{R_1}, \sigma_{R_1})$ is the reliability of the $MAD_{k,1}$. Unlike works that address the control with Z-numbers [43,45,46], we do

Table 1
Rule Table of *ZLSMC* ($\dot{s}$).

	$\dot{s}(t)$				
	NB, *S*	*NS*, *U*	*ZE*, *A*	*PS*, *U*	*PB*, *S*
$b(X,t) > 0$	$C_1 = NB, R_c$	$C_2 = NS, R_c$	$C_3 = ZE, R_c$	$C_4 = PS, R_c$	$C_5 = PB, R_c$
$b(X,t) < 0$	$C_1 = PB, R_c$	$C_2 = PS, R_c$	$C_3 = ZE, R_c$	$C_4 = NS, R_c$	$C_5 = NB, R_c$

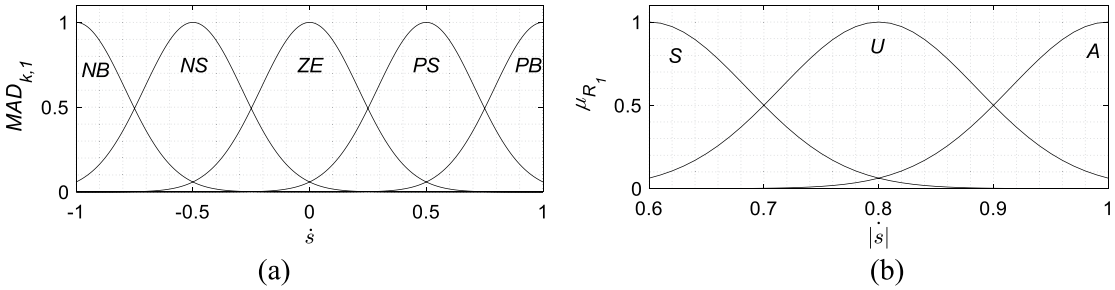

Fig. 1. (a) Membership functions for the MADs of $\dot{s}(t)$, (b) reliability of $|\dot{s}(t)|$ ($\sigma_{R_1} = 0.085$).

not define the reliability of the output, we compute its weight value as is proposed by [47]:

$$R_c = \frac{\int_0^1 |\dot{s}|\, \mu_{R1}(|\dot{s}|)}{\int_0^1 \mu_{R1}(|\dot{s}|)} \tag{20}$$

Now, it is used the weight of the reliability R_c and the value γ_k, in order to compute $TU(Z)$ of two singleton values as:

$$\gamma_{R_c}^k = \gamma_k \times R_c \tag{21}$$

And the output of the control action u_{nc}, based on (8) and (21), is:

$$u_{nc} = ZLSMC\,(s,\dot{s}) = \left| \frac{\arg\max(\gamma_k)}{\sum_{k=1}^m \gamma_k GAD_{k,\max(\bar{O})}} \right| \sum_{k=1}^m \gamma_{R_c}^k GAD_{k,\bar{O}} \tag{22}$$

To compute u_d, the selected Lyapunov function and its derivative are:

$$V(s(t)) = \frac{1}{2}s(t)^2 \tag{23}$$

$$\dot{V}(s(t)) = s(t)\dot{s}(t) \tag{24}$$

Replacing (17) in (24), and considering that $u = u_d$:

$$\begin{aligned} s(t)\dot{s}(t) = {} & s(t)\dot{x}_{dn}(t) - s(t)A\,(X,t) \\ & - s(t)b\,(X,t)\,u_d - s(t)d(t) \\ & + s(t)\sum_{i=1}^{n} r_{n-i}\lambda^i e^{(n-i)} < 0 \end{aligned} \tag{25}$$

Five classes are set for both inputs $\dot{s}(t)$ and $s(t)$ based on the scalability analysis presented in [36], and three classes for the reliability, as presented in [43]. Due to the normalization of the classes is computed u_{nd}, so, are added the scaling gain k_2 at the input $s(t)$, and k_d at the output as:

$$u_d = k_d u_{nd} \quad \Longrightarrow \quad u_d = k_d ZLSMC\,(s,\dot{s})\,; \quad k_d > 0 \tag{26}$$

For u_d is addressed the case $b(X,t) > 0$ since in the opposite case ($b(X,t) < 0$), only the sign of the classes changes in the restriction part, as detailed in the definition of rules of Table 1. The centers of the Z-classes are presented in Table 2, considering $C_k = (\gamma_k, R_d)\,, \forall k = \{1, 2, \ldots, 25\}$.

For the computation of u_d, the classes per descriptor and the membership functions of the reliability are presented in Fig. 2. Note that for the reliability part, the absolute values of $\dot{s}$ and s are measured, since we consider giving more weight when $|\dot{s}|$ and $|s|$ are far from zero. The functions assigned for $\dot{s}$ have been presented in Fig. 1, and for s are presented in Fig. 2.

The discontinuous control action of ZLSMC requires two descriptors as LAMDA inputs. (2) is computed for s and its derivative, that is, $j = 1$ for $\dot{s}$ and $j = 2$ for s. Then, the calculation of the new class centers is made based on the $TU_{k,j}(Z)$ as:

$$TU_{k,1}(Z) = TU\left(MAD_{k,1}, R_1\right) = \frac{\rho_{k,1} c_{R_1}}{\left(1 + 8{\sigma_{k,1}}^2\right)\left(1 + 8{\sigma_{R_1}}^2\right)} \tag{27}$$

$$TU_{k,2}(Z) = TU\left(MAD_{k,2}, R_2\right) = \frac{\rho_{k,2} c_{R_2}}{\left(1 + 8{\sigma_{k,2}}^2\right)\left(1 + 8{\sigma_{R_2}}^2\right)} \tag{28}$$

To compute the reliability at the output, we compute the weight value as proposed [47]:

$$R_d = \text{argmax}\left(\frac{\int_0^1 |\dot{s}|\, \mu_{R1}(|\dot{s}|)}{\int_0^1 \mu_{R1}(|\dot{s}|)}, \frac{\int_0^1 |s|\, \mu_{R2(|S|)}}{\int_0^1 \mu_{R2(|S|)}} \right) \tag{29}$$

The argmax function is used to obtain a more aggressive control action if the surface or its derivative are far from zero to carry the system faster towards the reference.

For the rules definition in Table 2, the following analysis has been considered:

- If $s(t) > 0$ and u_d increases, then the product $s(t)\dot{s}(t)$ decreases and vice-versa.
- If $s(t) < 0$ and u_d increases, then the product $s(t)\dot{s}(t)$ increases; and if u_d decreases, then $s(t)\dot{s}(t)$ decreases.

Based on the analysis presented above, the controller generates a control action u_d to satisfy $s(t)\dot{s}(t) < 0$ all the time. As has been described for the u_c, the discontinuous control action is similar. That is, *S* is associated as reliability to classes *PB* and *NB*, *U* to classes *PS* and *NS*, and *A* to class *ZE*, to generate abrupt control actions when the surface and its derivative are far from the desired value, and smooth control actions when they are close to zero.

From (21), it is used the weight of the reliability R_d and the values γ_k. The Total Utility of the Z-number at the output (composed of singleton values) is:

$$\gamma_{R_d}^k = \gamma_k \times R_d \tag{30}$$

Then, the output of the control action u_{nd}, based on (8) and (30), is:

$$u_{nd} = ZLSMC\,(s,\dot{s}) = \left| \frac{\arg\max(\gamma_k)}{\sum_{k=1}^m \gamma_k GAD_{k,\max(\bar{O})}} \right| \sum_{k=1}^m \gamma_{R_d}^k GAD_{k,\bar{O}} \tag{31}$$

Table 2
Rule table of Z-LSMC for *ZLSMC* $(s, \dot{s})$.

		$\dot{s}(t)$				
		NB, *S*	*NS*, *U*	*ZE*, *A*	*PS*, *U*	*PB*, *S*
$s(t)$	*PB*, *S*	$C_5 = ZE, R_d$	$C_{10} = ZE, R_d$	$C_{15} = PS, R_d$	$C_{20} = PB, R_d$	$C_{25} = PB, R_d$
	PS, *U*	$C_4 = ZE, R_d$	$C_9 = ZE, R_d$	$C_{14} = PS, R_d$	$C_{19} = PB, R_d$	$C_{24} = PB, R_d$
	ZE, *A*	$C_3 = NB, R_d$	$C_8 = NS, R_d$	$C_{13} = ZE, R_d$	$C_{18} = PS, R_d$	$C_{23} = PB, R_d$
	NS, *U*	$C_2 = NB, R_d$	$C_7 = NB, R_d$	$C_{12} = NS, R_d$	$C_{17} = ZE, R_d$	$C_{22} = ZE, R_d$
	NB, *S*	$C_1 = NB, R_d$	$C_6 = NB, R_d$	$C_{11} = NS, R_d$	$C_{16} = ZE, R_d$	$C_{21} = ZE, R_d$

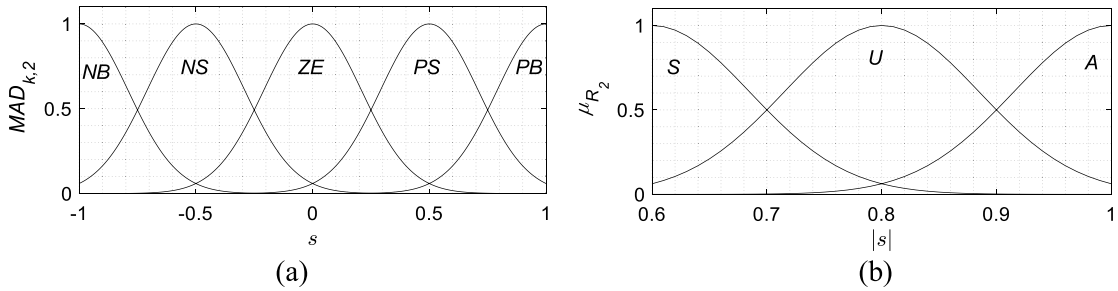

Fig. 2. (a) Membership functions for the MADs of $s(t)$, (b) reliability of $|s(t)|$ ($\sigma_{R_2} = 0.085$).

Then, the complete ZLSMC output is computed as:

$$u = k_c ZLSMC\ (\dot{s}) + k_d ZLSMC\ (s, \dot{s}) \tag{32}$$

2.3. Adaptive LAMDA control

This algorithm has been formalized in detail in [35], and it is focused on the modeling and control systems whose model is imprecise or unknown. Adaptive LAMDA works like a regressor considering an online self-adjustment of its internal parameters using a different learning method. Five layers are implemented for this objective:

Layers 1 and 2 calculate the MAD and GAD, respectively. The GADs normalization is computed in Layer 3 as:

$$NGAD_{k,\bar{O}} = \frac{GAD_{k,\bar{O}}}{\sum_{k=1}^{m} GAD_{k,\bar{O}}} \tag{33}$$

In Layer 4 are multiplied the $NGAD_{\bar{O},k}$ with a first-order T–S (Takagi–Sugeno) function $H_k(\cdot)$. These values are the consequent parameters. Thus:

$$\begin{aligned} &H_k\left(\bar{O}, h_{k1}, \ldots, h_{kj}, \ldots, h_{kn}, h_k\right) \\ &= \bar{o}_1 h_{k1} + \cdots + \bar{o}_j h_{kj} + \cdots + \bar{o}_n h_{kn} + h_k \end{aligned} \tag{34}$$

And the output of layer 4 is:

$$f_k = NGAD_{k,\bar{O}} H_k \tag{35}$$

Layer 5 is the sum of the values of layer 4:

$$Out_L = f_1 + \cdots + f_k + \cdots f_m \tag{36}$$

The proposed model (33)–(36) employs a hybrid learning algorithm to adjust the exigency, the antecedent, and the consequent parameters.

2.3.1. Hybrid learning algorithm (HLA)

HLA [48] is implemented to self-adjust the premise and consequent of the Adaptive LAMDA. The algorithm involves a step forward and a step backward, to improve the learning machine time [49].

- Forward pass:
- In this step, the antecedent coefficients $\theta = \{\rho_{k,j}, \sigma_{k,j}, \alpha\}$ are fixed, and the algorithm goes forward. In this step, the RLSE method adjusts the consequent parameters considering that $H_k(\cdot)$ is linear. For all the "d" desired values at the output $Out = \left[Out^1 \cdots Out^d \cdots Out^D\right]^T$ this process is carried out. For more detail see [35]. Backward pass

Considering that Out_L^d is the output of the Adaptive LAMDA corresponding to the individual $Out^d(k)$. Then, the error at the output of Layer 5 is:

$$E_d(k) = \frac{1}{2}\left[Out^d(k) - Out_L^d(k)\right]^2 \tag{37}$$

The goal is to spread backward $E_d(k)$ towards $\theta = \left\{\rho_{k,j}, \sigma_{k,j}, \alpha\right\}$. The correction of θ at the time $(k+1)$ with the Gradient Descent (GD) is calculated as:

$$\Delta\theta(k) = -\eta \frac{\partial E_d(k)}{\partial \theta(k)} \tag{38}$$

$$\begin{aligned} \theta\ (k+1) &= \theta(k) + \Delta\theta(k) + \beta\ (\theta(k) - \theta\ (k-1)) \\ &= \theta(k) - \eta \frac{\partial E_d}{\partial \theta} + \beta\ (\theta(k) - \theta\ (k-1)) \end{aligned} \tag{39}$$

where η is the learning rate, and $\beta \in [0, 1]$ is the coefficient of momentum.

The self-adjustment of the antecedent parameters with GD is summarized as:

$$\frac{\partial E_d}{\partial Out_L^d} = -\left(Out^d - Out_L^d\right) \tag{40}$$

$$\frac{\partial Out_L^d}{\partial f_k} = 1 \tag{41}$$

$$\frac{\partial f_k}{\partial NGAD_{\bar{X},k}} = H_k; \quad \forall k = 1, \ldots, m \tag{42}$$

$$\frac{\partial NGAD_{\bar{O},k}}{\partial GAD_{\bar{O},k_2}} = \begin{cases} \dfrac{\left(\sum_{k_2=1}^{m} GAD_{\bar{O},k_2}\right) - GAD_{\bar{O},k_2}}{\left(\sum_{k_2=1}^{m} GAD_{\bar{O},k_2}\right)^2} & if:\ k_2 = k \\ -\dfrac{GAD_{\bar{O},k}}{\left[\sum_{k=1}^{m} GAD_{\bar{O},k_2}\right]^2} & if:\ k_2 \neq k \end{cases} \tag{43}$$

$$\begin{aligned} \frac{\partial GAD_{\bar{O},k}}{\partial MAD_{k,j}} &= \alpha T\left(MAD_{k,1}, \ldots, MAD_{k,j_1}, \ldots, MAD_{k,n}\right) + (1-\alpha) \\ &\times \left(1 - S\left(MAD_{k,1}, \ldots, MAD_{k,j_1}, \ldots, MAD_{k,n}\right)\right); \\ &\forall j_1 \neq j \end{aligned} \tag{44}$$

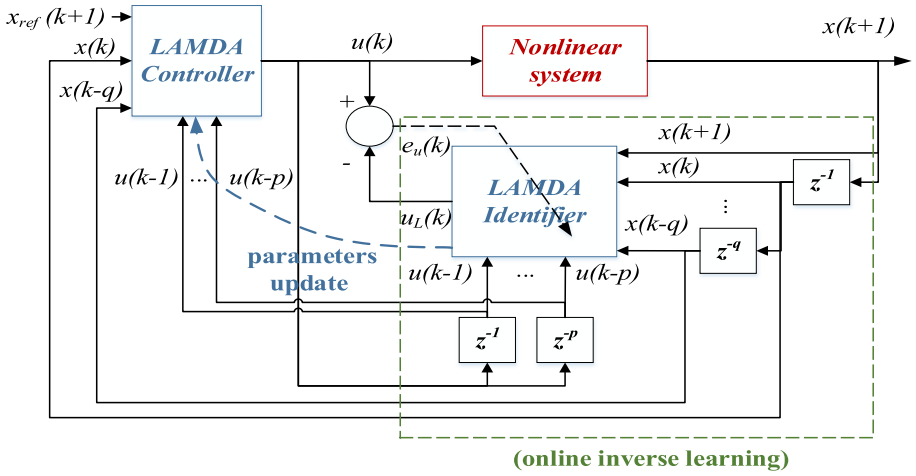

Fig. 3. Application stage of the inverse LAMDA control [35].

$$\frac{\partial MAD_{k,j}}{\partial \rho_{k,j}} = \frac{\left(\bar{x}_j - \rho_{k,j}\right)}{\left(\sigma_{k,j}\right)^2} \partial MAD_{k,j} \tag{45}$$

$$\frac{\partial MAD_{k,j}}{\partial \sigma_{k,j}} = \frac{\left(\bar{x}_j - \rho_{k,j}\right)^2}{\left(\sigma_{k,j}\right)^3} \partial MAD_{k,j} \tag{46}$$

$$\frac{\partial GAD_{\bar{O},k}}{\partial \alpha} = T\left(MAD_{k,1}, \ldots, MAD_{k,j}, \ldots, MAD_{k,n}\right) - S\left(MAD_{k,1}, \ldots, MAD_{k,j}, \ldots, MAD_{k,n}\right) \tag{47}$$

In [35] is detailed the computational complexity and the convergence of Adaptive LAMDA.

In the first stage, Adaptive LAMDA requires offline learning, which implies the application of a random input $u(k) = Out$ (the desired value at the output of LAMDA) to the system using the output $x(k+1) = o(k+1)$, its previous values, and the delayed values of $u(k)$ as input descriptors. Note that the nomenclature $o(k)$ corresponds to the descriptors used by LAMDA that correspond to the outputs of the system, so $o(k) = u(k)$.

In the application stage, the feedback closed loop shown in Fig. 3 is proposed. In the scheme, the identifier is trained online. Then, a duplicate LAMDA model is employed as controller.

The information on Adaptive LAMDA control here has been summarized so as not to lengthen the content of the paper. For more details on the learning mechanism, please review [35].

3. HVAC models

In this section, we present the HVAC models taken from the literature to test our LAMDA control approaches. The purpose of this work is not to evaluate the HVAC models used in the paper, which have been used in many references to test control approaches, such as [50–57]. We have used these HVAC models to validate our LAMDA-based controllers in terms of the transient and steady-state behaviors, control performances, and disturbance rejection.

3.1. Case study 1: MIMO HVAC

HVAC systems are structures with many elements that together are complex to accurately model. The first case study corresponds to a MIMO (Multiple-Input Multiple-Output) system with nonlinear characteristics presented in [50]. We have taken this HVAC model assuming that the system is operating on the cooling mode to validate our LAMDA-based controllers by using simulation tools. The characteristics that make an interesting

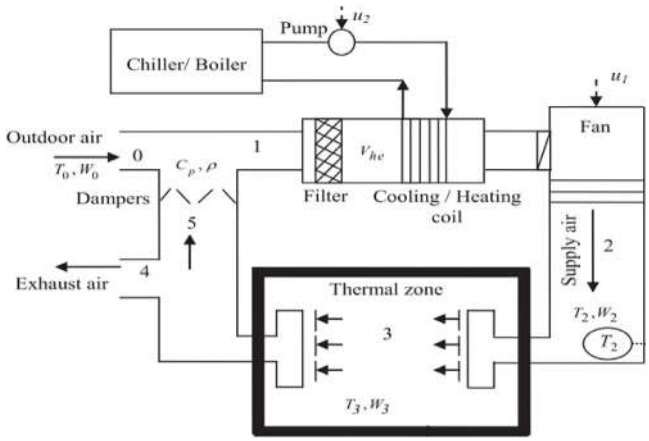

Fig. 4. Block diagram of a simple HVAC system [50].

study model of this system is that it has two output variables to control in the Thermal Zone of Fig. 4, which are: Temperature (T_3 [°F]) and Humidity Ratio (W_3 [lb/lb]), which are related to each other considering that the signals that control the pump and the fan are available as inputs.

In Fig. 4, the outdoor air flows inside the system mixing 25% of it with 75% of the returning air, ejecting the rest (0.25 and 0.75 are the coefficients of the initial conditions shown in (48)–(50)). The air mixture goes through the filter to the heat exchanger, where it is conditioned to the desired value. The conditioned air is propelled to the desired thermal zone with a fan. The system controls the parameters T_3 and W_3, based on the thermal loads of the Thermal Zone. The differential equations of energy and mass balances of the MIMO HVAC are:

$$\dot{T}_3 = \frac{f}{V_s}(T_2 - T_3) - \frac{h_{fg}}{C_p V_s}(W_s - W_3) + \frac{1}{0.25 C_p V_s}\left(Q_0 - h_{fg} M_0\right) \tag{48}$$

$$\dot{W}_3 = \frac{f}{V_s}(W_s - W_3) + \frac{M_0}{\rho V_s} \tag{49}$$

$$\dot{T}_2 = \frac{f}{V_{he}}(T_3 - T_2) - \frac{0.25f}{V_{he}}(T_0 - T_3) - \frac{f h_w}{C_p V_{he}}(0.25W_0 + 0.75W_3 - W_s) - 6000\frac{gpm}{\rho C_p V_{he}} \tag{50}$$

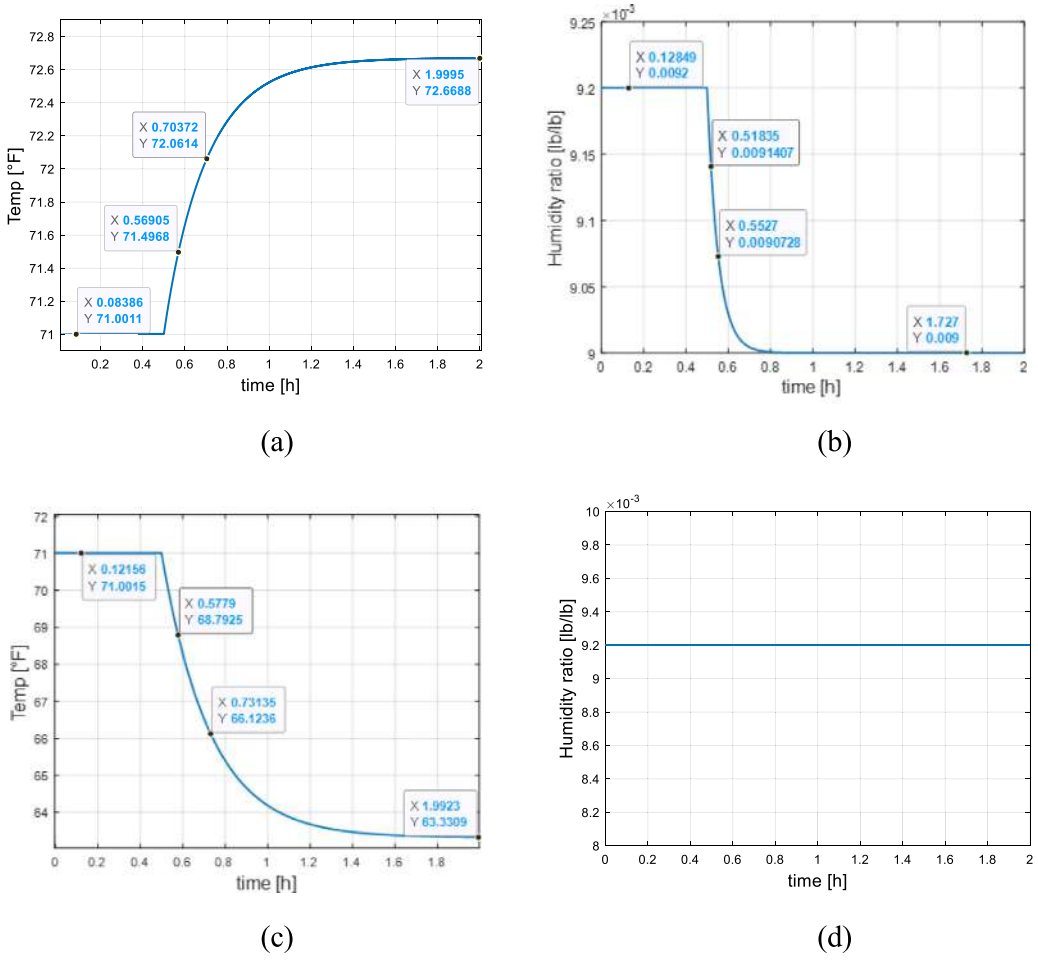

Fig. 5. (a) Response in x_1 as a consequence of 10% step change in u_1 (b) Response in x_2 as a consequence of 10% step change in u_1, (c) Response in x_1 as a consequence of a 10% step change in u_2, (d) Response in x_2 as a consequence of a 10% step change in u_2.

W_0 is the humidity ratio of the outdoor air, h_w is the enthalpy of the water, h_{fg} is the enthalpy of water vapor, V_{he} is the volume of the heat exchanger, C_p is the specific heat of air, $W_s = W_2$ is the humidity ratio of supply air, W_3 is the humidity ratio of thermal Zone 3, T_0 is the temperature of the outdoor air, M_0 is the moisture load, Q_0 is the sensible heat load, T_2 is the temperature of supply air, T_3 is the temperature of the thermal Zone 3, V_s is the volume of Zone 3, ρ is the air mass density, f is the volumetric flow rate of air (ft^3/min), and gpm is the flow rate of chilled water (gal/min).

Representing the system in state space, we consider $u_1 = f$, $u_2 = gpm$, $x_1 = T_3$, $x_2 = W_3$, $x_3 = T_2$, $y_1 = T_3$, $y_2 = W_3$. The following equalities are used to represent the model: $\alpha_1 = 1/V_s$, $\alpha_2 = h_{fg}/C_pV_s$, $\alpha_3 = 1/\rho C_pV_s$, $\alpha_4 = 1/\rho V_s$, $\beta_1 = 1/V_{he}$, $\beta_2 = 1/\rho C_pV_{he}$, $\beta_3 = h_w/C_pV_{he}$, Eqs. (48)–(50) are re-written as:

$$\dot{x}_1 = u_1\alpha_1 60\,(x_3 - x_1) - u_1\alpha_2 60\,(W_s - x_2) + \alpha_3\left(Q_0 - h_{fg}M_0\right) \quad (51)$$

$$\dot{x}_2 = u_1\alpha_1 60\,(W_s - x_2) + \alpha_4 M_0 \quad (52)$$

$$\dot{x}_3 = u_1\beta_1 60\,(x_1 - x_3) + u_1\beta_1 15\,(T_0 - x_1) - u_1\beta_3 60\,(0.25W_0 + 0.75x_2 - W_s) - 6000u_2\beta_2 \quad (53)$$

Tables 3 and 4 contain the numerical values and the system parameters at the operating point, respectively.

Tables 3 and 4 present values measured at the operating point $W_3 = 0.0092$ [lb/lb] and $T_3 = 71$ [°F], detailed in [50].

Table 3
Numerical values of the system parameters.

$W_{3ref} = 0.0088$ [lb/lb]	$V_{he} = 60.75$ [ft^3]	$V_s = 58,464$ [ft^3]
$\rho = 0.0074$ [lb/ft^3]	$C_p = 0.24$ [Btu/lb°F]	$f_{ref} = 17,000$ [ft^3/min]
$T_{ref} = 55$ [°F]	$T_{3ref} = 71$ [°F]	$W_s = 0.007$ [lb/lb]

Table 4
Numerical values of the system parameters at the operating point.

$u_1^0 = 17,000$ [ft^3/min]	$u_2^0 = 58$ [gpm]	$Q_0^0 = 289897.52$ [Btu/hr]
$x_1^0 = 71$ [°F]	$x_2^0 = 0.0092$ [lb/lb]	$x_3^0 = 55$ [°F]
$T_0^0 = 85$ [°F]	$W_0^0 = 0.0018$ [lb/lb]	$M_0^0 = 166.06$ [lb/hr]

Previously, we analyzed if a decoupling stage in the system is required to implement controllers for each variable independently. The reaction curve method was used in order to identify the input–output correlation to obtain the transfer functions. The procedure to obtain the transfer functions is detailed in [33].

Figs. 5.a and 5.b shows the HVAC responses with a step signal applied only to the volumetric flow rate of air "u_1", and Figs. 5.c and 5.d show the HVAC responses with a step signal applied only to the flow rate of chilled water "u_2". The responses are similar to first-order plus dead time (FOPDT) models parametrized as [58]:

$$\frac{X(s)}{U(s)} = \frac{Ke^{-tos}}{\tau s + 1} \quad (54)$$

where K is the gain of the system, t_o is the dead time, and τ is the time constant.

As Fig. 5 shows, u_1 affects the variables Temperature and Humidity Ratio, while a variation of u_2 only affects the Temperature.

Using the reaction curve method for identification, and the linearized model $G(s)$ considering the four transfer functions obtained by the identification applied in Fig. 5, we have:

$$Y(s) = G(s)U(s) \tag{55}$$

$$G(s) = \begin{bmatrix} g_{11} & g_{12} \\ g_{21} & g_{22} \end{bmatrix} = \begin{bmatrix} \dfrac{9.8164 \times 10^{-4} e^{-0.0016}}{0.2137\ \mathrm{s} + 1} & \dfrac{-1.3223 e^{-0.0012\ \mathrm{s}}}{0.2301\ \mathrm{s} + 1} \\ \dfrac{-1.1764 \times 10^{-7} e^{-0.0011\ \mathrm{s}}}{0.0527\ \mathrm{s} + 1} & 0 \end{bmatrix} \tag{56}$$

From (56), the gain matrix K is:

$$K = \begin{bmatrix} 9.8164 \times 10^{-4} & -1.3223 \\ -1.1764 \times 10^{-7} & 0 \end{bmatrix} \tag{57}$$

The Bristol's matrix or relative gain array RGA [59] is used to evaluate the input–output interaction, and is defined as:

$$RGA(K) = \Lambda(K) \triangleq K \times \left(K^{-1}\right)^T \tag{58}$$

The operator $\times$ represents the element-by-element multiplication:

$$\Lambda(K) = \begin{bmatrix} \lambda_{11} & \lambda_{12} \\ \lambda_{21} & \lambda_{22} \end{bmatrix} = \begin{bmatrix} 0 & 1 \\ 1 & 0 \end{bmatrix} \tag{59}$$

The matrix $\Lambda(K)$ represents the inputs–outputs dependence, proving that the decoupling stage is not required. Therefore, the two independent LAMDA controllers implementation for the temperature and humidity ratio is possible.

$$u_2 \rightarrow x_1 \ and \ u_1 \rightarrow x_2 \tag{60}$$

The parameter identification performed in Fig. 5 gives the following values for the Humidity Ratio: $K_W = -1.3223$, $\tau_W = 0.2301$ s, $t_{0W} = 0.0012$ s, and for Temperature: $K_T = -1.1764 \times 10^{-7}$, $\tau_T = 0.0527$ s, $t_{0T} = 0.0011$ s, being the transfer functions:

$$G_1 = \frac{x_2}{u_1} = \frac{-1.1764 \times 10^{-7} e^{-0.0011\ \mathrm{s}}}{0.0527\ \mathrm{s} + 1}; \quad G_2 = \frac{x_1}{u_2} = \frac{-1.3223 e^{-0.0012\ \mathrm{s}}}{0.2301\ \mathrm{s} + 1} \tag{61}$$

3.1.1. LAMDA-PID applied to the MIMO hvac

With the knowledge of the approximate model, it is proposed the LAMDA-PID design [33]. The controllers inputs are e_T, $\dot{e}_T$, e_W and $\dot{e}_W$, with e as the error and $\dot{e}$ as its derivative. These variables are chosen to drive the HVAC system to the desired zero states, where the temperature and humidity ratio errors and their derivatives are zero.

In Fig. 6 are presented the centers of classes C_k and the γ_k values, in order to represent the expression that synthesizes the fuzzy logic inference mechanism detailed in (6). Must be considered that these 25 classes are the training data for LAMDA operation; and also are defined for each controller, setting the centers as a combination of the following sets:

$$e_W = [-1, -0.5, 0, 0.5, 1]\ [\mathrm{lb/lb}], \quad \text{and} \quad \dot{e}_W = [-1, -0.5, 0, 0.5, 1]\ \left[\frac{\mathrm{lb/lb}}{\mathrm{h}}\right] \tag{62}$$

$$e_T = [-1, -0.5, 0, 0.5, 1]\ [^\circ\mathrm{F}], \quad \text{and} \quad \dot{e}_T = [-1, -0.5, 0, 0.5, 1]\ \left[\frac{^\circ\mathrm{F}}{\mathrm{h}}\right] \tag{63}$$

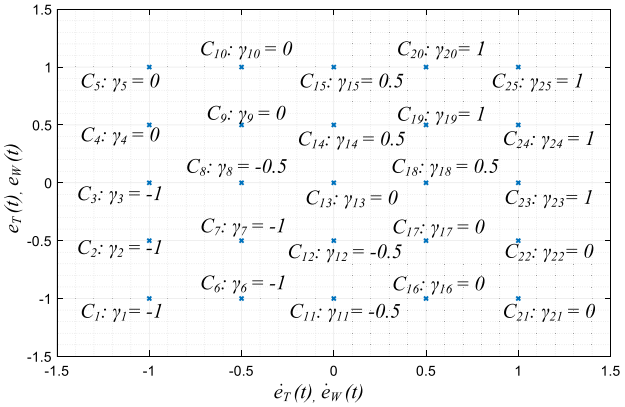

Fig. 6. Defined classes and outputs for the humidity ratio and temperature.

The LAMDA-PID calculates the output $\left[u_W(t) \quad u_T(t)\right]^T$ required to bring the system to the desired set point. The structure of the controller is shown in Fig. 7. The scheme shows blocks with the scaling gains $kp_1 = 200$, $kd_1 = 10$, $ki_1 = 3 \times 10^5$, $kp_2 = 0.1$, $kd_2 = 0.01$ and $ki_2 = 330$ for tuning the controllers response, which have been empirically calibrated with the ISE (Integral Square Error) minimization method.

3.1.2. ZLSMC applied to the MIMO HVAC

The LSMC design for the humidity ratio and the temperature is similar. For ease of design, LSMC uses the linearized model based on the approximation of Eq. (61). Thus, to summarize the design stage, only the temperature procedure is detailed.

Consider the FOPTD expression (54) for the Temperature:

$$\frac{X_T(s)}{U_T(s)} = \frac{K_T e^{-t_{0T} s}}{\tau_T s + 1} \tag{64}$$

Modeling of the dead time t_{0T} with a first-order Taylor series approximation [58]:

$$e^{-t_{0T} s} \cong \frac{1}{t_{0T} s + 1} \tag{65}$$

Substituting (65) into (64):

$$\frac{X_T(s)}{U_T(s)} \cong \frac{K_T}{\tau_T t_{0T} s^2 + (\tau_T + t_{0T}) s + 1} \tag{66}$$

Re-writing (66) in the time domain:

$$\tau_T t_{0T} \ddot{x}_T + (\tau_T + t_{0T}) \dot{x}_T + x_T - K_T u_T = 0 \tag{67}$$

The state-space system representation is:

$$\dot{x}_{T1} = x_{T2}$$
$$\dot{x}_{T2} = -\frac{(\tau_T + t_{0T})}{\tau_T t_{0T}} x_{T2} - \frac{1}{\tau_T t_{0T}} x_{T1} + \frac{K_T}{\tau_T t_{0T}} u_T \tag{68}$$

Where $x_{T1} = x_T$

The form of (67) is similar to (8). So, the procedure for designing a stable ZLSMC controller presented in Section 2.2 is feasible.

As shown (67), the system is a second-order model, thus $n = 2$. The sliding surface for the temperature $s_T(t)$ is defined as:

$$s_T(t) = \dot{e}_T(t) + 2\lambda e_T(t) + \lambda^2 \int e_T(t) dt \tag{69}$$

The derivative of (69) is:

$$\dot{s}_T(t) = \ddot{e}_T(t) + 2\lambda \dot{e}_T(t) + \lambda^2 e_T(t) = 0 \tag{70}$$

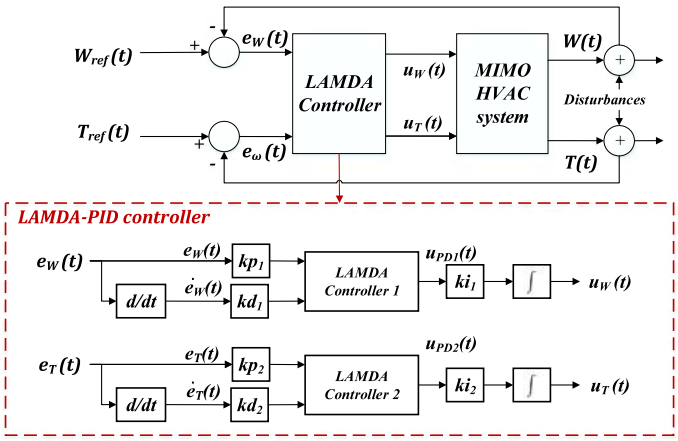

Fig. 7. Control scheme for the regulation of the MIMO HVAC System with LAMDA-PID.

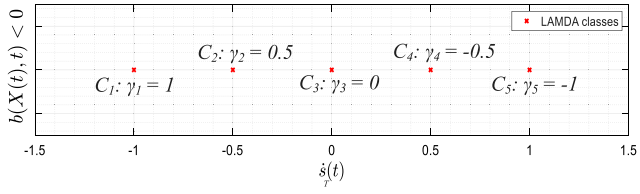

Fig. 8. Rules and classes for u_{cT} based on $\dot{s}_T(t)$.

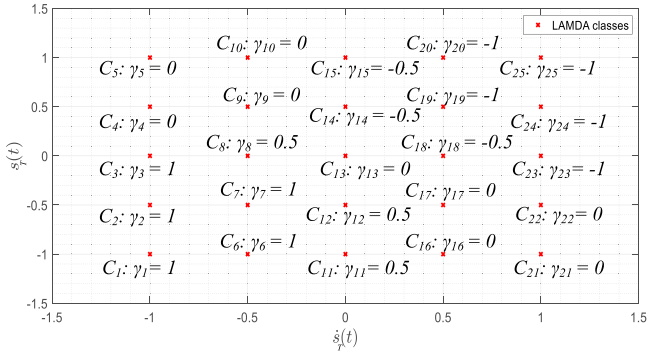

Fig. 9. Rules and Classes for u_{dT} based on $\dot{s}_T(t)$ and $s_T(t)$.

taking into consideration $n = 2$ in (15):

$$\ddot{e}_T(t) = \dot{x}_{dT2}(t) - \dot{x}_{T2}(t) \tag{71}$$

Thus, replacing (68) and (71) in (70):

$$\dot{s}(t) = \dot{x}_{dT2}(t) + \frac{(\tau_T + t_{0T})}{\tau_T t_{0T}} x_{T2} + \frac{1}{\tau_T t_{0T}} x_{T1} - \frac{K_T}{\tau_T t_{0T}} u_T + 2\lambda \dot{e}_T(t) + \lambda^2 e_T(t) = 0 \tag{72}$$

The parameters identification has shown that $(K_T/\tau_T t_{0T}) < 0$. Thus, based on (8), it is concluded that $b(X,t) < 0$. Therefore, we use the rules of Table 1. Table 2 requires a sign change as mentioned in Section 2.2. The continuous control action based on the classes established is shown in Fig. 8. For example, if $\dot{s}_T(t) = 0.5$, then the Class 2 is activated, resulting in $u_{ncT} = -0.5$ to satisfy $\dot{s}(t) = 0$.

The classes defined in the discontinuous control action are shown in Fig. 9. For example, if $\dot{s}_T(t) = 0.5$ and $s(t) = 1$, then Class 20 is activated, resulting in a control action $u_{ndT} = -1$ to satisfy $s(t)\dot{s}(t) < 0$.

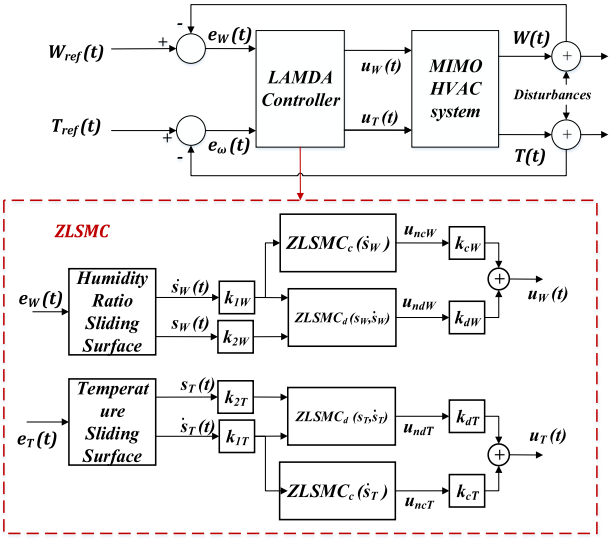

Fig. 10. Control scheme for the regulation of the MIMO HVAC System with ZLSMC.

The block diagram of the proposed LSMC controller is presented in Fig. 10, where two ZLSMC controllers are applied to regulate the MIMO HVAC system.

The blocks shown in the scheme are with the scaling gains $k_{1W} = 2.5$, $k_{2W} = 2.5 \times 10^{-5}$, $k_{cW} = 0.01$, $k_{dW} = 3 \times 10^6$, $k_{1T} = 0.2$, $k_{2T} = 2.5 \times 10^{-4}$, $k_{cT} = 5$, and $k_{dT} = 20$, for tuning the controllers response, which have been empirically calibrated with the ISE minimization method.

3.1.3. Adaptive LAMDA on the MIMO HVAC

The system is discretized to test Adaptive LAMDA, and the scheme of the controller is presented in Fig. 11. LAMDA Identifier 1 uses two inputs $[W(k+1); W(k)]$ because it is a first-order plant. In this work, two classes have been considered for each input with the following values: $\eta_1 = 0.02$, $\beta_1 = 0.01$, $\lambda_1 = 0.997$. LAMDA Identifier 2 uses two inputs $[T(k+1); T(k)]$, each with two classes. The internal parameters are: $\eta_2 = 0.95$, $\beta_2 = 0.01$, $\lambda_2 = 0.997$. The simulation sampling time is $T_s = 1.2$ min. For training, some random inputs are generated with 60 steps of 54 min duration.

The LAMDA Identifier 1 is placed between the control action u_W and the output of the Humidity Ratio W in order to learn the inverse model of the system. To minimize the error

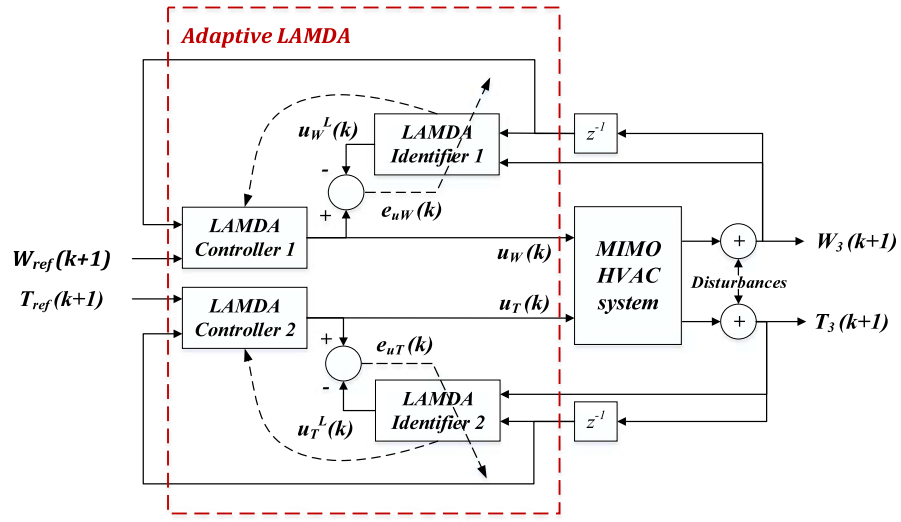

Fig. 11. Control scheme for the regulation of the MIMO HVAC System with Adaptive LAMDA.

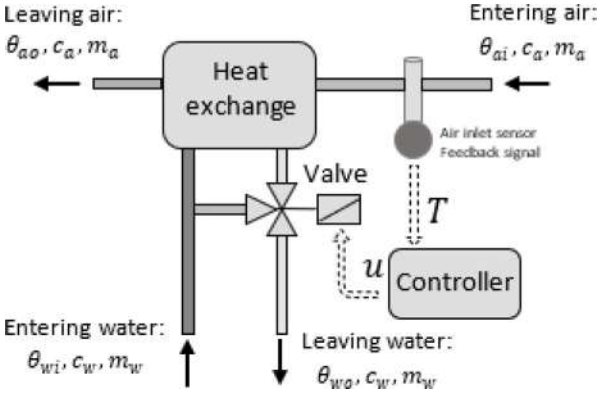

Fig. 12. General scheme of the HVAC-WDT model [57].

$e_{uW}(k) = u_W(k) - u_W^L(k)$, the output W and its previous states are used as inputs for the identifier, where u_W^L is the output of the LAMDA identifier 1. The minimization of $e_{uW}(k)$ allows the self-adjustment of the internal coefficients of LAMDA, which are updated at every sample time. This procedure is applied in the same way to the temperature T, minimizing the error $e_{uT}(k) = u_T(k) - u_T^L(k)$.

3.2. Case study 2: HVAC with dead time (HVAC-WDT)

This case study is widely detailed in [57], and it is interesting due to the dead time presented at the system output caused by the dynamics of the heat exchanger, actuators, valves and sensors. Fig. 12 shows the HVAC-WDT model, where inlet hot water heats up the inlet air, which provokes a change in the outlet air temperature. The modeling explanation is divided into three parts: the valve subsystem, the heat transfer subsystem, and the complete open-loop plant.

The heat transfer is assumed like a continuously stirred tank, where its input variables are: $\theta_{wo}, m_w, \theta_m$, which represents water temperature output [°C], water mass flow rate [Kg $\times$ s^{-1}] and the heat exchanger material temperature [°C], respectively. The Output of the system is represented by U_w and U_a, which are the water and air thermal transmission coefficient in [W $\times$ m^{-2} $\times$ K^{-1}]. Moreover, U_w equations depend on the laminar or turbulent forced convection related to the Reynold number Re. Finally, the equations of U_w and U_a are:

$$U_{w1} = \left(5.823 + 1.153 \times 10^{-1} \times \theta_{wo} - 1.48 \times 10^{-4} \times {\theta_{wo}}^2\right) \times \left(\frac{m_w}{n_t {d_i}^{2.25}}\right)^{0.8} \rightarrow R_e \geq 2300 \quad (73)$$

$$U_{w2} = \frac{4.36}{di} * \left(5.702 \times 10^{-1} + 1.79 \times 10^{-3} \times \bar{\theta}_{wm} - 6.7714 \times 10^{-6} \times \bar{\theta}_{wm}^2\right) \rightarrow R_e < 2300 \quad (74)$$

$$U_a = 60.37 + 140.3e^{\left(\frac{28.62-\theta_m}{9.796}\right)} \quad (75)$$

where: $\bar{\theta}_{wm} = \frac{\theta_{wo}+\theta_m}{2}$, $n_t = 10, d_i = 0.0117$ [m], $U_w = \max(U_{w1}|_{Re\geq 2300}, U_{w2}|_{Re<2300})$

The valve and its actuator are represented by a first-order model, where the input is the control signal u and the output characteristic is represented as ψ (see Eq.(76)). Moreover, could be considered two behaviors related with its inherent characteristic, γ: percentage valve (see Eq. (77)) and linear valve (see (78)), where, $N = 0.371$, and $f_0 = 0.045$.

$$\psi = \gamma\left(\gamma^2(1-N) + N\right)^{-1/2} \quad (76)$$

$$\gamma = {f_0}^{(1-u)} \quad (77)$$

$$\gamma = f_0 + u(1-f_0) \quad (78)$$

The other equations of the complete model are:

$$\theta_{wo} = \int \left(\frac{1}{C_w} m_w c_w (\theta_{wi} - \theta_{wo}) - q_w\right) dt \quad (79)$$

$$q_w = U_w A_w (\theta_{wo} - \theta_m) \quad (80)$$

$$\theta_m = \int \frac{1}{C_m}(q_w - q_a)\, dt \quad (81)$$

$$q_a = U_a A_a (\theta_m - \theta_{ao}) \quad (82)$$

$$\theta_{ao} = \frac{m_a c_a \theta_{ai} + U_a A_a \theta_m}{m_a c_a + U_a A_a} \quad (83)$$

$$m_w = \int \frac{1}{\tau_a}(\psi m_{wd} - m_w)\, dt \quad (84)$$

$$T = \int \frac{1}{\tau_d}(\theta_{ao} - T)\, dt \quad (85)$$

Table 5
Simulation parameters and system initial conditions at the operating point.

$C_w = 4.836$ [kJ K^{-1}]	$C_m = 4.047$ [kj K^{-1}]	$c_a = 1.002$ [kJ kg^{-1}K^{-1}]
$c_w = 4.194$ [kJkg^{-1} K^{-1}]	$A_a = 5.181$ [m^2]	$\tau_d = 30$ [s]
$A_w = 0.404$ [m^2]	$m_a = 0.3144$ [kg s^{-1}]	$m_{wd} = 0.619$ [kg s^{-1}]
$\theta_{ao}(0) = \theta_{ai}(0) = 12$ [°C]	$\theta_m(0) = \theta_{ai}(0)$	$m_w = 0$
$\phi(0) = \theta_{ai}(0)$;	$\theta_{wi} = 50$ [°C]	

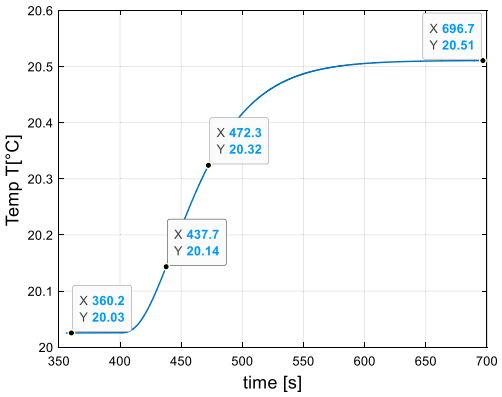

Fig. 13. (a) Response of Temperature T as a consequence of 10% step change in u.

Table 5 contain the system initial conditions and the numerical values for the simulation parameters.

In Fig. 13 is presented the HVAC-WDT responses with a step signal of 10% applied to the valve. The response is similar to the form presented in (63).

The parameter identification performed for Fig. 13 gives the following values: =19.51, $\tau = 51.9$ [s], $t_0 = 20.4$ [s], being the transfer function:

$$G(s) = \frac{x(s)}{u_T(s)} = \frac{19.51e^{-20.4s}}{51.9\ \mathrm{s} + 1} \tag{86}$$

As can be seen in (90), the dead time is almost half the plant time constant, which makes it an interesting system to test LAMDA controllers and their robustness to this parameter.

3.2.1. LAMDA-PID applied to the HVAC-WDT

Considering the approximate values of the model is designed the LAMDA-PID controller. The inputs of the controller are e_T, $\dot{e}_T$, where e is the error and $\dot{e}$ is its derivative, as shown in case study 1. The parameters in γ_k, and the centers of classes C_k are shown in Fig. 14, in order to represent the analytic expression that summarizes the fuzzy logic inference mechanism detailed in (7). 25 classes are defined for each controller, considering that they are the training data for LAMDA operation, where centers are configured as a combination of the following sets:

$$e_T = [-1, -0.5, 0, 0.5, 1]\ \ [^\circ\mathrm{C}], \quad \text{and}$$
$$\dot{e}_T = [-1, -0.5, 0, 0.5, 1]\ \left[\frac{^\circ\mathrm{C}}{\mathrm{s}}\right] \tag{87}$$

In order to bring the system to the desired reference, the controller computes the output $u_T(t)$. The proposed LAMDA-PID structure is shown in Fig. 15. The scheme shows the scaling gains $kp = 0.011$, $kd = 0.2$, $ki = 0.264$ for tuning the response of the controller, which has been empirically calibrated with the ISE minimization method.

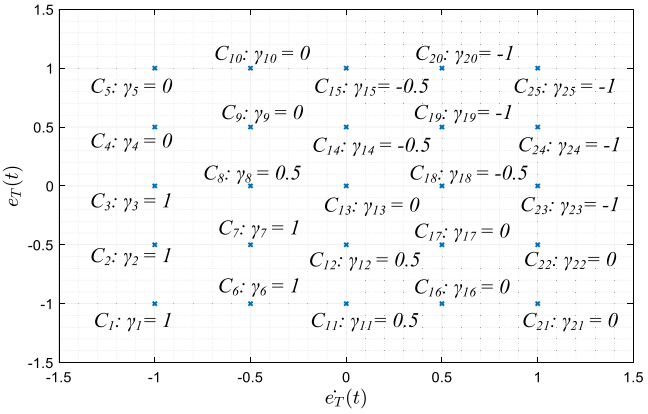

Fig. 14. Outputs and defined classes and for the temperature of HVAC-WDT.

3.2.2. ZLSMC applied to the HVAC-WDT

Considering the procedure from (64)–(67), the HVAC-WDT system can be represented as:

$$\frac{X(s)}{U(s)} \cong \frac{K}{\tau t_0 s^2 + (\tau + t_0)\, s + 1} \tag{88}$$

Solving (88) in the time domain:

$$\tau t_0 \ddot{x} + (\tau + t_0)\, \dot{x} + x - K u_T = 0 \tag{89}$$

The state-space system representation, with $x_1 = x$, is:

$$\begin{aligned} \dot{x}_1 &= x_2 \\ \dot{x}_2 &= -\frac{(\tau + t_0)}{\tau t_0} x_2 - \frac{1}{\tau t_0} x_1 + \frac{K}{\tau t_0} u_T \end{aligned} \tag{90}$$

The form of (90) is similar to (9). So, the procedure detailed in Section 2.2 for designing a stable ZLSMC controller is feasible. The order of the system is $n = 2$, as is defined in (90). Thus, the sliding surface for the temperature $s_T(t)$ is:

$$s_T(t) = \dot{e}_T(t) + 2\lambda e_T(t) + \lambda^2 \int e_T(t) dt \tag{91}$$

The derivative of (91) is:

$$\dot{s}_T(t) = \ddot{e}_T(t) + 2\lambda \dot{e}_T(t) + \lambda^2 e_T(t) = 0 \tag{92}$$

Replacing $n = 2$ in (16):

$$\ddot{e}_T(t) = \dot{x}_{d2}(t) - \dot{x}_2(t) \tag{93}$$

Moreover, replacing (93) and (90) in (92):

$$\begin{aligned} \dot{s}_T(t) = \dot{x}_{d2}(t) + \frac{(\tau + t_0)}{\tau t_0} x_2 + \frac{1}{\tau t_0} x_1 - \frac{K}{\tau t_0} u_T + 2\lambda \dot{e}_T(t) + \lambda^2 e_T(t) \\ = 0 \end{aligned} \tag{94}$$

The parameters identified previously demonstrate that $(K/\tau t_0) > 0$, and based on (9), it is concluded that $b\,(X, t) > 0$. Therefore, Tables 1 and 2 are used for the controller design. Fig. 16 shows the classes established for the continuous control action. For example, if $\dot{s}_T(t) = 0.5$, then the Class 2 is activated, resulting in a control action $u_{ncT} = 0.5$ to satisfy $\dot{s}(t) = 0$.

Fig. 17 shows the discontinuous control action classes. For example, if $\dot{s}_T(t) = 0.5$ and $s_T(t) = 1$, then Class 20 is activated, resulting in a control action $u_{ndT} = 1$ to satisfy $s_T(t)\dot{s}_T(t < 0)$.

The block diagram of ZLSMC applied to the HVAC-WDT is presented in Fig. 18. The scheme shows the scaling gains $k_{1T} = 0.9$, $k_{2T} = 0.05$, $k_{cT} = 0.5$, and $k_{dT} = 2$ for tuning the controllers response, which again, have been empirically calibrated with the ISE minimization method.

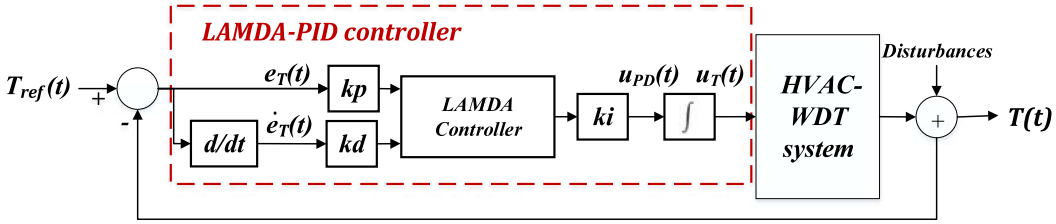

Fig. 15. Control scheme for the regulation of the HVAC-WDT System with LAMDA-PID.

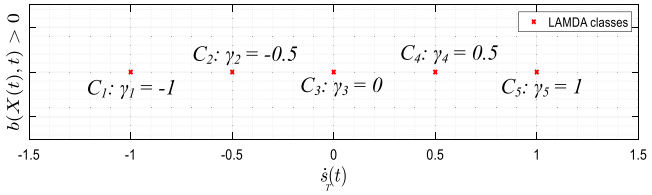

Fig. 16. Continuous control action u_{cT} based on $\dot{s}_T(t)$ with its Classes and rules.

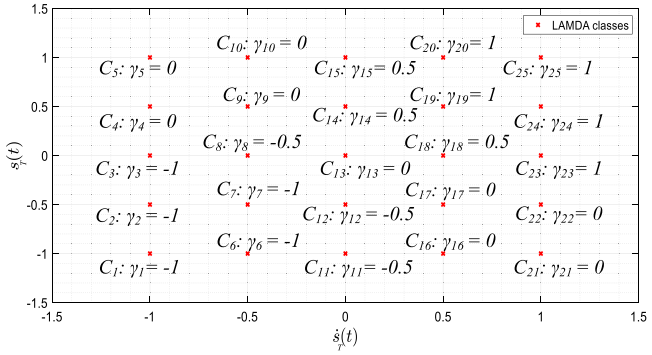

Fig. 17. Discontinuous control action u_{dT} based on $\dot{s}_T(t)$ and $s_T(t)$ with its Classes and rules.

3.2.3. Adaptive LAMDA applied to the MIMO HVAC

To work with Adaptive LAMDA, the system is discretized. LAMDA Identifier uses two inputs $[T(k+1); T(k)]$, each one with two classes. The design parameters are $\eta_2 = 0.99$, $\beta_2 = 0.01$, $\lambda_2 = 0.01$. The sampling period of the simulation is $T_s = 1$ [s]. Random inputs are generated and consist of 30 different values of 200 [s] duration.

In Fig. 19, in order to learn the inverse model of the system, the online LAMDA Identifier is placed between the control action u_T and the output Temperature T. To minimize the error $e_{uT}(k) = u_T(k) - u_T^L(k)$, the output T and its previous states are used as inputs for the identifier, where u_T^L is the output of the LAMDA identifier. The minimization of $e_{uT}(k)$ allows the adjusting of the LAMDA model parameters, which are updated in the controller at every sample time.

4. Simulations and results

The LAMDA control schemes performed in Section 2 are tested in regulation tasks of the HVAC systems shown in the case studies of Section 3. The controllers have been programmed and implemented in the Matlab (Simulink) software to validate their operation and performance. Five controllers are tested in all the experiments, these are: PID, Fuzzy-PID, LAMDA-PID, Adaptive LAMDA and ZLSMC. The LAMDA controllers have been calibrated as detailed in the previous section, minimizing the ISE, like the Fuzzy-PID, while the PID has been calibrated by the quarter decay ratio equations presented in [59].

4.1. Tests and results of case study 1

The performance of LAMDA controllers is evaluated under abrupt disturbances applied to the system in order to test the robustness (disturbance rejection). The index ISE is calculated in each controller and compared with conventional methods widely used in HVAC systems, as PID and Fuzzy PID. Disturbances of Heat and Humidity Ratio (see Fig. 20) are applied to the HVAC system independently, in order to observe the performance of each controller to regulate the desired variables of the Thermal Zone 3.

Specifically, the disturbances T_d and W_d affect the system in Eqs. (48)–(50) in the temperature T_3 and Humidity ratio W_3 as:

$$\dot{T}_3 = \frac{f}{V_s}(T_2 - (T_3 + T_d)) - \frac{h_{fg}}{C_p V_s}(W_s - (W_3 + W_d)) + \frac{1}{0.25 C_p V_s}\left(Q_0 - h_{fg} M_0\right) \tag{95}$$

$$\dot{W}_3 = \frac{f}{V_s}(W_s - (W_3 + W_d)) + \frac{M_0}{\rho V_s} \tag{96}$$

$$\dot{T}_2 = \frac{f}{V_{he}}((T_3 + T_d) - T_2) - \frac{0.25f}{V_{he}}(T_0 - (T_3 + T_d)) - \frac{f h_w}{C_p V_{he}}(0.25 W_0 + 0.75(W_3 + W_d) - W_s) - 6000\frac{gpm}{\rho C_p V_{he}} \tag{97}$$

Initially, only the temperature disturbance is considered in the HVAC system. Fig. 21 shows that u_1 stays at 17000 [cfm] (see Fig. 21.a), and the Humidity Ratio stays at 0.0092 [lb/lb] (see Fig. 21.b). Particularly, as explained in Section 3, the humidity ratio is not directly affected by temperature changes. For this reason, Fig. 21.b shows a constant response of this variable.

Fig. 22. a shows the control output u_2, and Fig. 22.b shows the behavior of the temperature T_3 in the case that the temperature disturbance is applied to the MIMO HVAC. As can be seen, the controllers stabilize and regulate the plant adequately. Analyzing qualitatively the control and Temperature signals, when is observed in detail the zoom of Fig. 22, it can be seen that ZLSMC presents the response that brings the system towards the reference the fastest, in a less abrupt way, and with fewer oscillations, unlike the other methods, especially PID. It is worth noting that the PID settling time-calibrated by the quarter decay ratio presented in [59] for the inset plot is 1.8 [h], a value much higher than that obtained by the proposals based on LAMDA. Specifically, ZLSMC with a settling time equal to 0.4 [h] represents a considerable improvement (around 450%).

Quantitatively, based on the ISE and ISCO (Integral Square Control Output), it can be determined which of the controllers is the best in terms of performance and energy consumption. These indices should be of a low value since the first shows how fast the controller reaches the reference and the second the energy required by the controller to stabilize the HVAC system. Fig. 23 shows a similar ISCO in all cases ($ISCO \approx 71000$), but

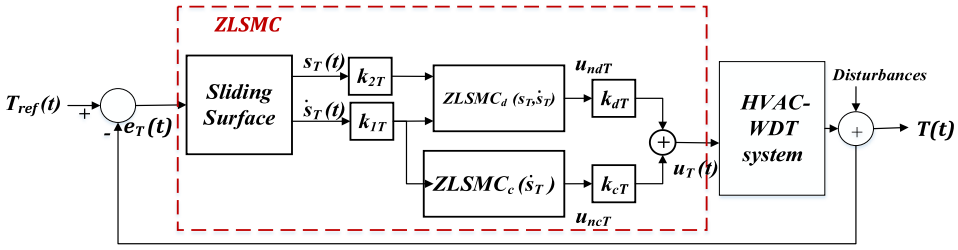

Fig. 18. Control scheme for the regulation of the HVAC-WDT System with ZLSMC.

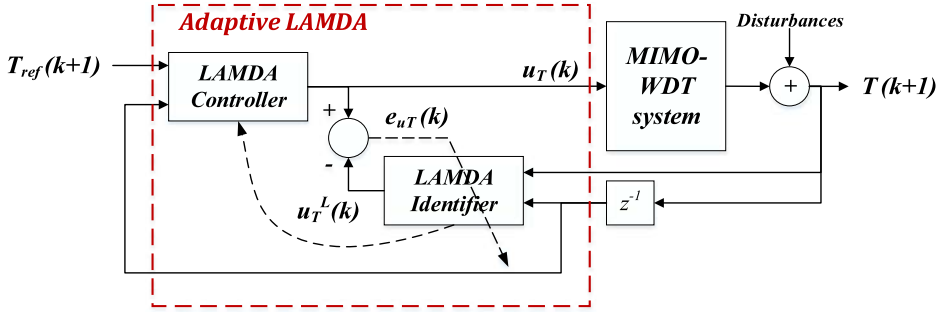

Fig. 19. Control scheme for the regulation of the HVAC-WDT System with Adaptive LAMDA.

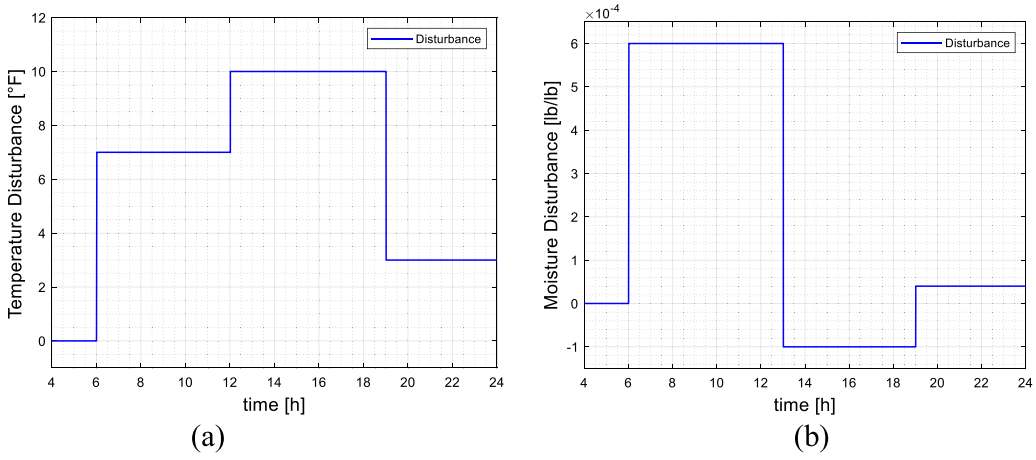

Fig. 20. (a) Heat disturbance T_d, and (b) Humidity disturbance W_d applied to the MIMO HVAC.

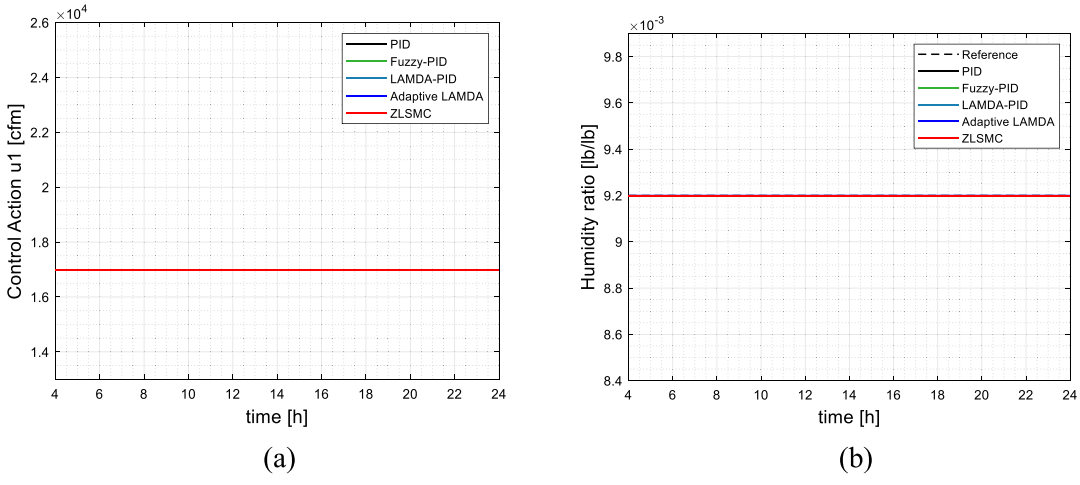

Fig. 21. Results of temperature disturbance applied to the MIMO HVAC: (a) control action u_1, (b) Humidity Ratio W_3.

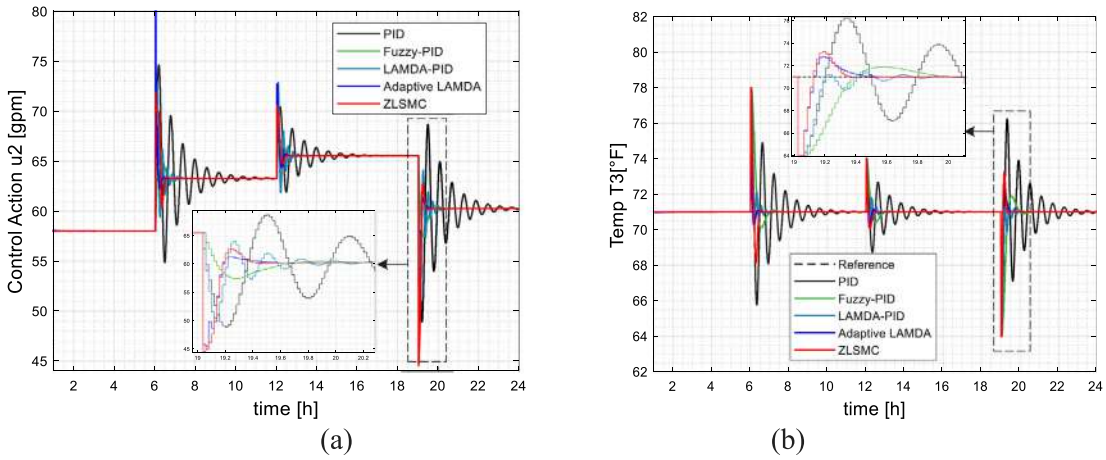

Fig. 22. Results of temperature disturbance applied to the MIMO HVAC: (a) control action u_2, (b) Temperature T_3.

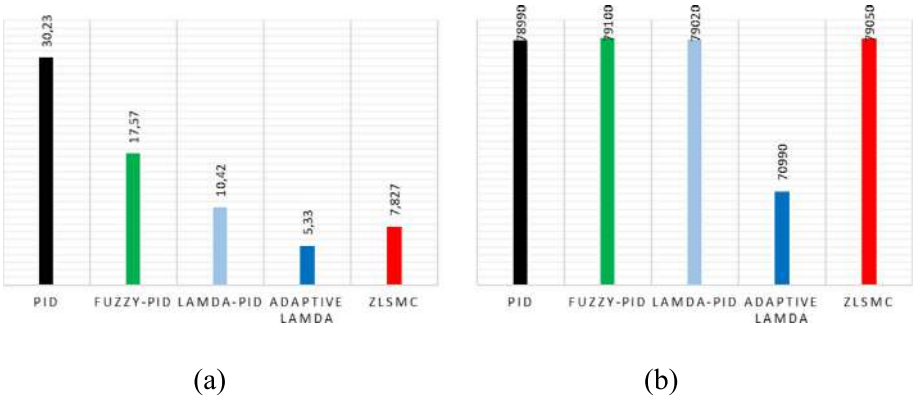

Fig. 23. Numerical values for (a) ISE and (b) ISCO for the MIMO HVAC with temperature disturbance.

the controller with lower ISE is adaptive LAMDA ($ISE_{ADAPTIVE} = 5.33$), that is, it is the best in terms of performance, followed by the ZLSMC ($ISE_{ZLSMC} = 7.827$). Fuzzy and PID have the worst performance indices. Based on these results, adaptive LAMDA and ZLSMC are suitable proposals for the control of the HVAC system when there are temperature disturbances. Thus, although the results are numerically similar for the case of ISCO, qualitatively it has been possible to observe a considerable improvement in the performance of adaptive LAMDA and ZLSMC with respect to the other proposals, especially, in the way the controllers carry the output of the system towards the reference.

In the next simulation, the humidity disturbance is applied to the MIMO HVAC to observe the behavior of variables T_3, W_3, and their corresponding controllers. Fig. 24.a shows the control action u_1, and Fig. 24.b shows the output Humidity Ratio W_3, Fig. 25.a the control action u_2, and Fig. 25.b the output of the Temperature T_3, for all the tested controllers.

Figs. 24 and 25 show that the humidity disturbance applied to the HVAC affects both controlled variables of the thermal zone, W_3 and T_3. For the Humidity Ratio (see Fig. 24), it can be seen that the outputs of the LAMDA methods are very good, the system reaches the reference during the simulation. Again, ZLSMC and Adaptive LAMDA present the best responses, presenting less fluctuations in the transient, and therefore, faster convergence to the reference. It is good to highlight that the non-adaptive methods for calibration have an extra complexity due to the interaction of the input–output variables, calibration that is not required by the Adaptive LAMDA method. The PID settling time in Fig. 25 is 0.5 [h], a value higher than that obtained by the ZLSMC, with a settling time equal to 0.2 [h], which represents an improvement of around 250%.

Fig. 25 shows that methods based on LAMDA regulate the Temperature T_3 in a good way. Control actions of PID and Fuzzy-PID are abrupt and oscillatory, which make them take longer to reach the reference. Again, ZLSMC and Adaptive LAMDA control are less abrupt than the other methods, stabilizing the HVAC system in a very short time, which is the goal of the control.

The quantitative analysis shown in Fig. 26 shows that the ISCO values are not significantly different in the two variables (about 7×10^9 humidity and 7×10^4 for temperature). However, in terms of ISE, it is shown that in the case of Humidity Ratio, Adaptive LAMDA is the best ($ISE_{ADAPTIVE} = 6.20 \times 10^{-8}$), followed by ZLSMC ($ISE_{ZLSMC} = 6.98 \times 10^{-8}$). For the temperature, ZLSMC is the best ($ISE_{ZLSMC} = 0.255$), followed by the adaptive proposal ($ISE_{ADAPTIVE} = 0.288$), besides, it is observed that PID and Fuzzy-PID decrease considerably in performance (see the abrupt oscillations), which indicates that they are not robust enough to reject humidity disturbances, and therefore, require recalibration of parameters. These results are consistent with the case in which a temperature disturbance is added. The fact that the control action in all cases has a similar ISCO means that the controllers use a similar amount of energy to reach the reference. However, the ISE index and the graphically observed response show that ZLSMC improves the behavior of the system and establishes itself in the reference in less time. Especially, when observing the ISE in the case of Temperature (Fig. 26.c), it is representatively better than that of conventional methods such as fuzzy and PID, which shows the advantage of the proposed method.

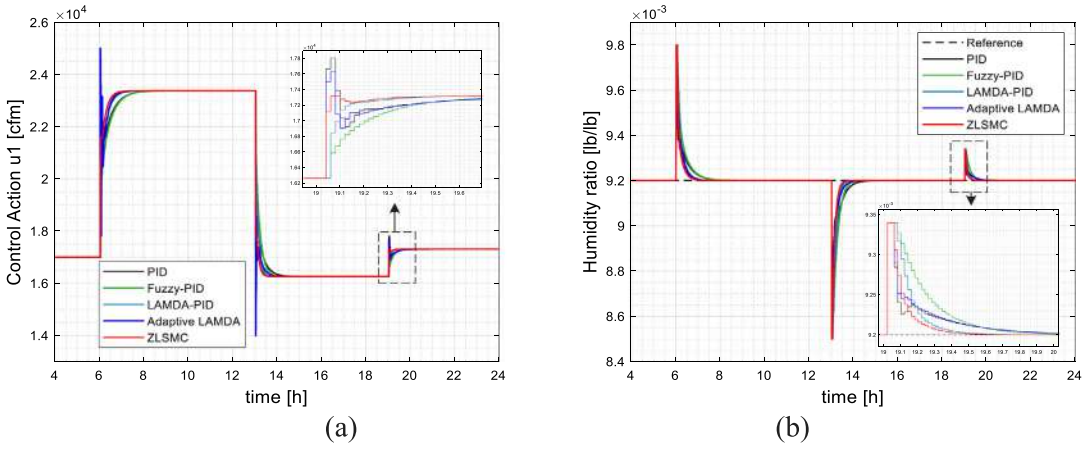

Fig. 24. Results of Humidity disturbance applied to the MIMO HVAC: (a) control action u_1, (b) Humidity Ratio W_3.

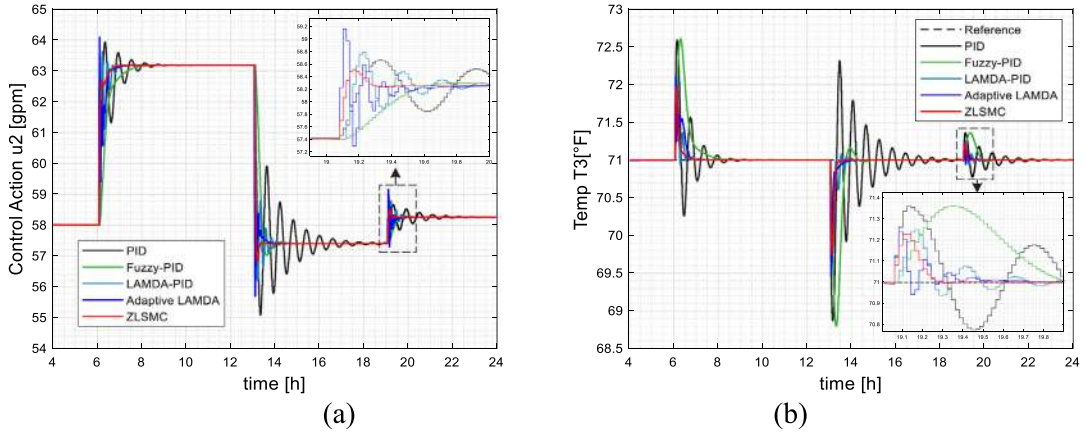

Fig. 25. Results of Humidity disturbance applied to the MIMO HVAC: (a) control action u_2, (b) Temperature T_3.

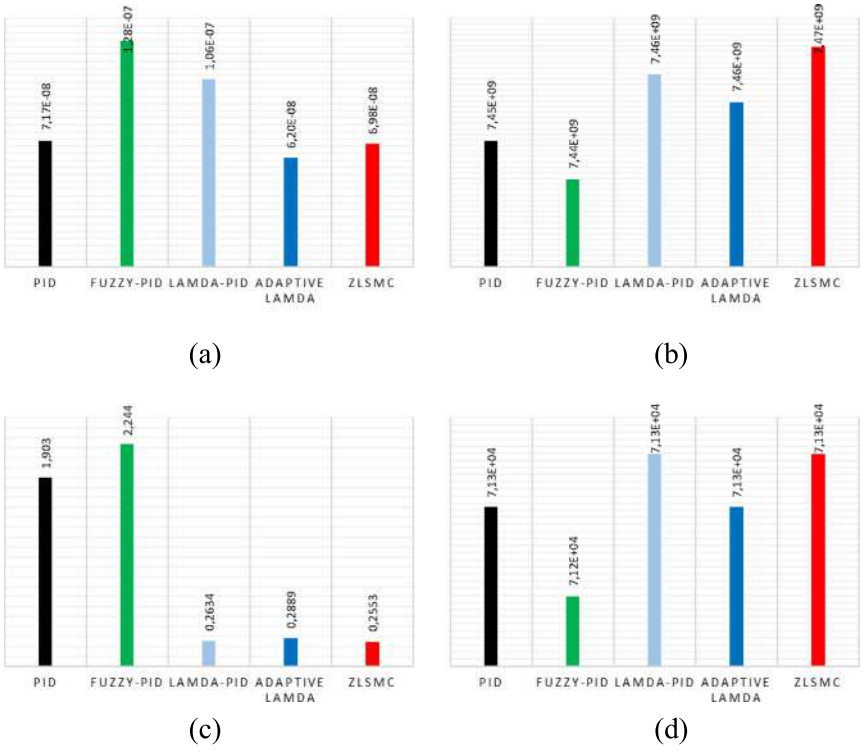

Fig. 26. Numerical values for (a) ISE and (b) ISCO of the Humidity Ratio, (c) ISE and (d) ISCO of the Temperature for the MIMO HVAC with humidity disturbance.

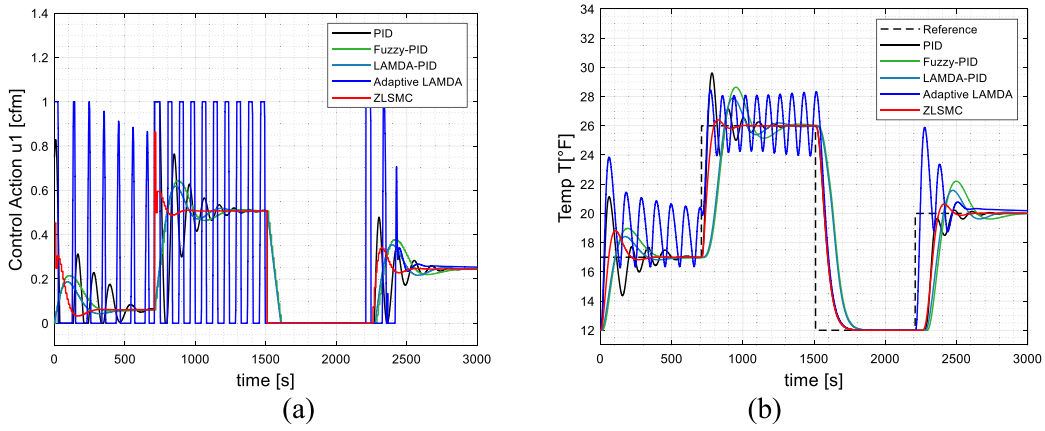

Fig. 27. Reference change of HVAC with dead time: (a) control action u_1, (b) Temperature T.

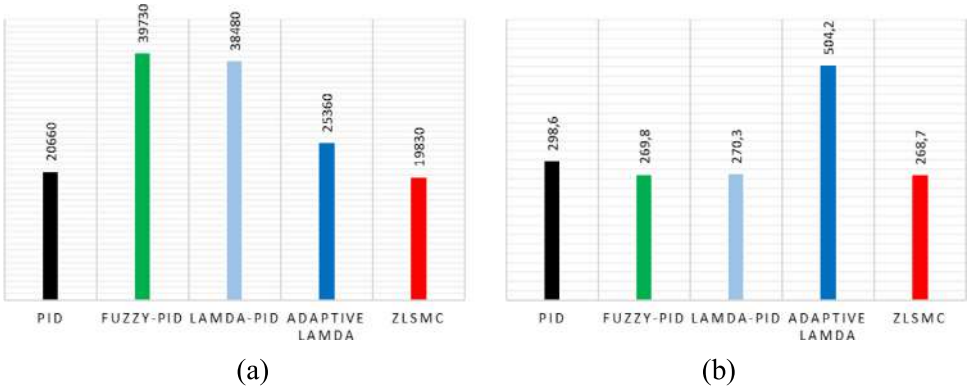

Fig. 28. Numerical values for (a) ISE and (b) ISCO for the HVAC with dead time under reference changes.

4.2. Tests and results of case study 2

The performance of LAMDA controllers is analyzed when the temperature reference is changed to step inputs (abrupt changes). The objective is to observe its response and the ability of the controllers to reach the reference and stabilize the system with a minimum power consumption control action. Fig. 27.a shows the control actions of each controller, and Fig. 27.b the output of the system. Qualitatively analyzing these signals, it is observed that the Adaptive LAMDA presents a highly oscillatory signal that at the end of the simulation stabilizes the system. This shows that this controller is not capable of controlling systems with excessive dead time ($t_0 \approx 20$ [s]). PID has been calibrated, as presented by Underwood [57], showing oscillatory responses like the Fuzzy PID, which stabilizes the system after a long period of time. The most adequate response is from ZLSMC, presenting minimum overshoot, reaching the reference effectively without an abrupt control action.

Quantitatively, Fig. 28 shows that, indeed, ZLSMC is the best proposal in terms of ISE ($ISE_{ZLSMC} = 19830$) and ISCO ($ISCO_{ZLSMC} = 268.7$). This means that it reaches the reference faster with the lowest energy consumption, which is desired in this type of system with dead time.

Finally, the performance of the controllers based on LAMDA is evaluated when the system is subjected to abrupt disturbances, in order to test disturbance rejection and robustness. Fig. 29.a shows the control actions in each controller, and Fig. 29.b the Temperature of the output of the system. The qualitative analysis of these signals shows that the PID, Fuzzy, LAMDA and ZLSMC controllers are capable of reaching effectively the reference, while the Adaptive LAMDA controller remains oscillatory with considerable steady-state errors, which demonstrates its degradation in processes with considerable dead time. It is evident that ZLSMC reaches the reference faster than the other methods, with less oscillation and overshoot.

The Adaptive LAMDA presents a highly oscillatory signal that fails to reach the reference, while the other proposals do it in a short time. From a quantitative point of view, Fig. 30 shows that, indeed, ZLSMC is the best proposal in terms of ISE ($ISE_{ZLSMC} = 19740$), with the second lowest value of ISCO ($ISCO_{ZLSMC} = 545.2$). LAMDA-PID presents the best value of ISCO ($ISCO_{LAMDA} = 526.7$); however, its ISE ($ISE_{LAMDA} = 45620$) is extremely high because it takes a long time to reach the reference.

It is evident that in this case study, the numerical results are quite similar. However, ZLSMC is always the lowest for the tests carried out. In order to discern which is better, we have relied on the qualitative analysis of Figs. 27 and 29, which clearly show that the proposals based on LAMDA are much better, in terms of fewer oscillations, response time and even over peak, which is the most appropriate in this type of HVAC system with time delay, and where the characteristics of the plant change when the operating point changes, varying the reference.

5. Conclusions

The LAMDA control approaches for the regulation of HVAC systems have been evaluated in this paper. As shown in the experiments, the system output converged towards the desired output for the first case study with all the controllers. The results have demonstrated that the proposals work quite well as

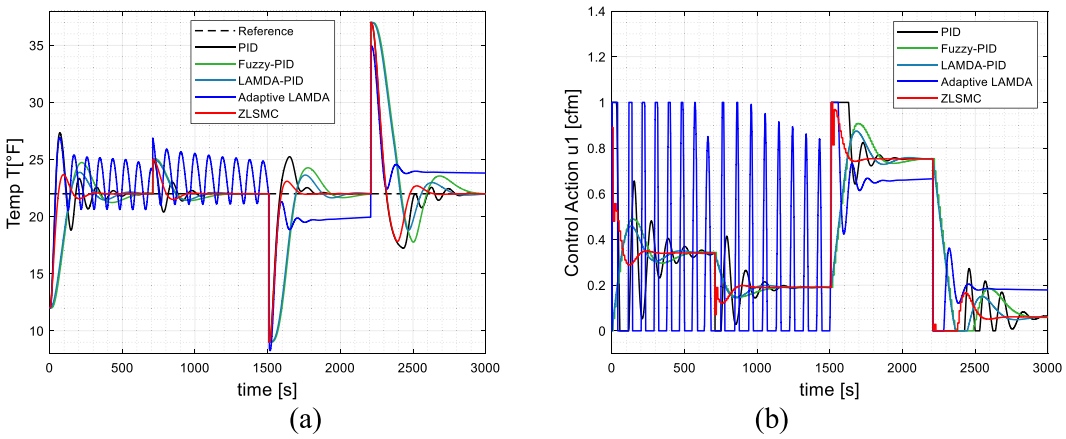

Fig. 29. Disturbances applied to the HVAC with dead time (a) control action u_1, (b) Temperature T.

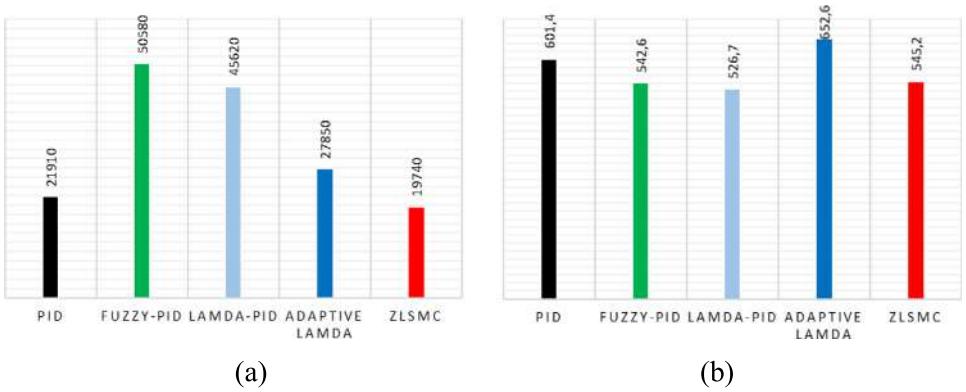

Fig. 30. Numerical values for (a) ISE and (b) ISCO for the HVAC with dead time under temperature disturbances.

independent controllers to control uncoupled MIMO systems, in which the results of ZLSMC and Adaptive LAMDA stand out. These controllers are the most efficient in terms of control action and performance. Also, the results show that ZLSMC is the most suitable since qualitatively and quantitatively it presents the best results with less oscillations, reaching the reference faster. Finally, potential improvements have been demonstrated in this work using LAMDA for MIMO HVAC systems, reducing the time of the system response and the energy consumption related to the control action applied to the actuators.

The second case study has shown that ZLSMC is the best controller in systems with representative dead time, a problem often found in modern HVAC systems due to the delay present in sensors and actuators. This case study has allowed us to observe that Adaptive LAMDA degrades its performance by not reaching the reference in the experiments carried out, which is logical since modeling these systems is not enough with learning algorithms working as regressors. Therefore, based on the analysis of other proposals, the use of predictors is required to improve performance.

Finally, LAMDA approaches are competitive, with better performance than conventional controllers, such as PID and Fuzzy-PID, methods generally used in HVAC systems, which are increasingly complex due to the large number of elements that compose them.

Future works must consider improvements in the Adaptive LAMDA approach for systems with dead time to prevent the controller degradation, since this is an interesting proposal because it does not require expert knowledge for its adjustment and calibration.

CRediT authorship contribution statement

L. Morales: Conceptualization, Methodology, Formal analysis, Simulations, Writing. **D. Pozo-Espín:** Conceptualization, Simulations, Writing. **J. Aguilar:** Conceptualization, Methodology, Writing, Supervision. **M.D. R-Moreno:** Supervision, Corrections, Funding acquisition.

Declaration of competing interest

The authors declare that they have no known competing financial interests or personal relationships that could have appeared to influence the work reported in this paper.

Acknowledgments

J Aguilar has received funding from the European Union's Horizon 2020 research and innovation programme under the Marie Skłodowska-Curie grant agreement No 754382 GOT ENERGY TALENT. M.D. R-Moreno is supported by the JCLM project SBPLY/19/180501/000024 and the Spanish Ministry of Science and Innovation project PID2019-109891RB-I00, both under the European Regional Development Fund (FEDER).

References

[1] J. Son, H. Kim, Sensorless air flow control in an HVAC system through deep learning, Appl. Sci. 9 (16) (2019).
[2] Qurat-Ul-Ain, S. Iqbal, S.A. Khan, A.W. Malik, I. Ahmad, N. Javaid, IoT operating system based fuzzy inference system for home energy management system in smart buildings, Sensors 18 (9) (2018) 1–30.

[3] G. Halhoul Merabet, et al., Intelligent building control systems for thermal comfort and energy-efficiency: A systematic review of artificial intelligence-assisted techniques, Renew. Sustain. Energy Rev. 144 (2021).
[4] M. Esrafilian-Najafabadi, F. Haghighat, Occupancy-based HVAC control systems in buildings: A state-of-the-art review, Build. Environ. 197 (2021).
[5] J. Rehrl, D. Schwingshackl, M. Horn, A modeling approach for HVAC systems based on the LoLiMoT algorithm, IFAC 19 (3) (2014).
[6] Z. Afroz, G.M. Shafiullah, T. Urmee, G. Higgins, Modeling techniques used in building HVAC control systems: A review, Renew. Sustain. Energy Rev. 83 (October) (2018) 64–84.
[7] R.Z. Homod, Review on the HVAC system modeling types and the shortcomings of their application, J. Energy 2013 (2013) 1–10.
[8] A. Almabrok, M. Psarakis, A. Dounis, Fast tuning of the PID controller in an HVAC system using the Big Bang-Big Crunch algorithm and FPGA technology, Algorithms 11 (10) (2018).
[9] M. Dey, M. Gupta, S.P. Rana, M. Turkey, S. Dudley, A PID inspired feature extraction method for HVAC terminal units, in: 2017 IEEE Conference on Technologies for Sustainability, SusTech 2017, vol. 2018, 2018, pp. 1–5.
[10] M. Soufiane, B. Imane, R. Ikram, B. Fatah, D. Belkacem, Modeling and Control Thermal of Building for Improve Comfort Level By using PID and On/Off Methods in the Case South-West Algeria, vol. 35, 2018.
[11] T.I. Salsbury, J.M. House, C.F. Alcala, Decoupling method for PI controllers via setpoint modification applied to HVAC systems, in: ASME 2018 Dynamic Systems and Control Conference, DSCC 2018, vol. 2, 2018.
[12] N. Sundriyal, P. Yadav, M. Chaturvedi, A Novel Approach for Designing PID Controller for Set-Point Tracking for a HVAC Process, vol. 479, 2017.
[13] C. Anastasiadi, A.I. Dounis, Co-simulation of fuzzy control in buildings and the HVAC system using BCVTB, Adv. Build. Energy Res. 12 (2) (2018) 195–216.
[14] A. Berouine, et al., A fuzzy logic-based approach for HVAC systems control, in: 2019 6th International Conference on Control, Decision and Information Technologies, CoDIT 2019, 2019, pp. 1510–1515.
[15] A. Suliman, R. Uskenbayeva, A. Altayeva, Applying Neuro-Fuzzy model in indoor comfort microclimate control, in: 2020 8th International Conference on Information Technology and Multimedia, ICIMU 2020, 2020, pp. 177–182.
[16] A. Parisio, D. Varagnolo, M. Molinari, G. Pattarello, L. Fabietti, K.H. Johansson, Implementation of a scenario-based MPC for HVAC systems: An experimental case study, IFAC 19 (3) (2014).
[17] M. Gholamzadehmir, C. Del Pero, S. Buffa, R. Fedrizzi, N. Aste, Adaptive-predictive control strategy for HVAC systems in smart buildings – A review, Sustain. Cities Soc. 63 (2020).
[18] G. Lymperopoulos, P. Ioannou, Building temperature regulation in a multi-zone HVAC system using distributed adaptive control, Energy Build. 215 (2020).
[19] A. Shah, D. Huang, T. Huang, Dynamic modelling and multivariable control of buildings climate by using sliding mode control, in: Proceedings of 2020 IEEE International Conference on Artificial Intelligence and Information Systems, ICAIIS 2020, 2020, pp. 552–555.
[20] Y. Yang, G. Hu, C.J. Spanos, Stochastic optimal control of HVAC system for energy-efficient buildings, IEEE Trans. Control Syst. Technol. (2021).
[21] Y. Li, Z. O'Neill, A critical review of fault modeling of HVAC systems in buildings, Build. Simul. 11 (5) (2018) 953–975.
[22] M.S. Mirnaghi, F. Haghighat, Fault detection and diagnosis of large-scale HVAC systems in buildings using data-driven methods: A comprehensive review, Energy Build. 229 (2020).
[23] A. Rogers, F. Guo, B. Rasmussen, Uncertainty analysis and field implementation of a fault detection method for residential HVAC systems, Sci. Technol. Built Environ. 26 (3) (2020) 320–333.
[24] X. Dai, J. Liu, X. Zhang, A review of studies applying machine learning models to predict occupancy and window-opening behaviours in smart buildings, Energy Build. 223 (2020).
[25] T. Hong, Z. Wang, X. Luo, W. Zhang, State-of-the-art on research and applications of machine learning in the building life cycle, Energy Build. 212 (2020).
[26] Y. Du others, Intelligent multi-zone residential HVAC control strategy based on deep reinforcement learning, Appl. Energy 281 (2021).
[27] X. Ding, W. Du, A.E. Cerpa, MB2C: Model-based deep reinforcement learning for multi-zone building control, in: BuildSys 2020 - Proceedings of the 7th ACM International Conference on Systems for Energy-Efficient Buildings, Cities, and Transportation, 2020, pp. 50–59.
[28] R.-E. Tudoroiu, M. Zaheeruddin, S.M. Radu, N. Tudoroiu, The MATLAB/SIMULINK implementation of a single zone temperature control strategies, in: Proceedings of the 6th International Conference on Inventive Computation Technologies, ICICT 2021, 2021, pp. 317–323.
[29] Z. Afroz, G.M. Shafiullah, T. Urmee, G. Higgins, Modeling techniques used in building HVAC control systems: A review, Renew. Sustain. Energy Rev. 83 (2018) 64–84.
[30] Y. Chen, S. Treado, Development of a simulation platform based on dynamic models for HVAC control analysis, Energy Build. 68 (PARTA) (2014) 376–386.
[31] N. Mendes, G.H.C. Oliveira, H.X. Araújo, L.S. Coelho, A MATLAB-based simulation tool for building thermal performance analysis, in: Eighth Int. IBPSA Conf, 2003, pp. 855–862.
[32] L. Yu, et al., Multi-agent deep reinforcement learning for HVAC control in commercial buildings, IEEE Trans. Smart Grid 12 (1) (2021) 407–419.
[33] L. Morales, J. Aguilar, A. Garces-Jimenez, J.A. Gutierrez De Mesa, J.M. Gomez-Pulido, Advanced fuzzy-logic-based context-driven control for HVAC management systems in buildings, IEEE Access 8 (2020) 16111–16126.
[34] L. Morales, J. Aguilar, A. Rosales, J.A.G. de Mesa, D. Chavez, An intelligent controller based on LAMDA, in: 2019 IEEE 4th Colombian Conference on Automatic Control, CCAC, 2019, pp. 1–6.
[35] L. Morales, J. Aguilar, A. Rosales, D. Chávez, P. Leica, Modeling and control of nonlinear systems using an adaptive LAMDA approach, Appl. Soft Comput. 95 (2020).
[36] L. Morales, J. Aguilar, O. Camacho, A. Rosales, An intelligent sliding mode controller based on LAMDA for a class of SISO uncertain systems, Inf. Sci. 567 (2021) 75–99.
[37] F. Ruiz, C. Isaza, A. Agudelo, J. Agudelo, A new criterion to validate and improve the classification process of LAMDA algorithm applied to diesel engines, Eng. Appl. Artif. Intell. 60 (2016) (2017) 117–127.
[38] L. Morales, J. Aguilar, A. Rosales, D. Pozo-Espin, A fuzzy sliding-mode control based on Z-numbers and LAMDA, IEEE Access PP (2021) 1.
[39] J. Waissman, R. Sarrate, T. Escobet, J. Aguilar, B. Dahhou, Wastewater treatment process supervision by means of a fuzzy automaton model, in: IEEE International Symposium on Intelligent Control, 2000, pp. 163–168.
[40] L. Morales, C. Ouedraogo, J. Aguilar, C. Chassot, S. Medjiah, K. Drira, Experimental comparison of the diagnostic capabilities of classification and clustering algorithms for the QoS management in an autonomic IoT platform, Serv. Orient. Comput. Appl. 13 (2019) 199–219.
[41] M. Sugeno, T. Takagi, Fuzzy identification of systems and its applications to modeling and control, IEEE Trans. Syst. Man Cybern. 15 (1) (1985) 116–132.
[42] J.-J. Slotine, W. Li, Applied NoLinear Optimal Control, Prentice Hall, New Jersey, 1991.
[43] R.H. Abiyev, N. Akkaya, I. Gunsel, Control of omnidirectional robot using z-number-based fuzzy system, IEEE Trans. Syst. Man Cybern. 49 (1) (2019) 238–252.
[44] B. Kang, Y. Deng, R. Sadiq, Total utility of Z-number, Appl. Intell. 48 (3) (2018) 703–729.
[45] R.H. Abiyev, Z number based fuzzy inference system for dynamic plant control, Adv. Fuzzy Syst. 2016 (2016).
[46] M. Abdelwahab, V. Parque, A.M.R. Fath Elbab, A.A. Abouelsoud, S. Sugano, Trajectory tracking of wheeled mobile robots using Z-number based fuzzy logic, IEEE Access 8 (2020) 18426–18441.
[47] B. Kang, D. Wei, Y. Li, Y. Deng, A method of converting Z-number to classical fuzzy number, J. Inf. Comput. Sci. 9 (3) (2012) 703–709.
[48] M.A. Shoorehdeli, M. Teshnehlab, A.K. Sedigh, Training ANFIS as an identifier with intelligent hybrid stable learning algorithm based on particle swarm optimization and extended Kalman filter, Fuzzy Sets and Systems 160 (7) (2009) 922–948.
[49] M.A. Shoorehdeli, M. Teshnehlab, A.K. Sedigh, M.A. Khanesar, Identification using ANFIS with intelligent hybrid stable learning algorithm approaches and stability analysis of training methods, Appl. Soft Comput. 9 (2) (2009) 833–850.
[50] B. Arguello-Serrano, M. Velez-Reyes, Nonlinear control of a heating, ventilating, and air conditioning system with thermal load estimation, IEEE Trans. Control Syst. Technol. 7 (1) (1999) 56–63.
[51] C. Zhang, S.R. Kuppannagari, R. Kannan, V.K. Prasanna, Building HVAC scheduling using reinforcement learning via neural network based model approximation, in: BuildSys 2019 - Proc. 6th ACM Int. Conf. Syst. Energy-Efficient Build. Cities, Transp, 2019, pp. 287–296.
[52] Zhang Huaguang, Lilong Cai, Decentralized nonlinear adaptive control of an HVAC system, IEEE Trans. Syst. Man Cybern. C 32 (4) (2002) 493–498.
[53] G. Jahedi, M.M. Ardehali, Wavelet based artificial neural network applied for energy efficiency enhancement of decoupled HVAC system, Energy Convers. Manage. 54 (1) (2012) 47–56.
[54] C. Rentel-Gómez, M. Vélez-Reyes, Decoupled control of temperature and relative humidity using a variable-air-volume HVAC system and non-interacting control, in: IEEE Conf. Control Appl. - Proc, 2001, pp. 1147–1151.
[55] E. Semsar-Kazerooni, M.J. Yazdanpanah, C. Lucas, Nonlinear control and disturbance decoupling of HVAC systems using feedback linearization and backstepping with load estimation, IEEE Trans. Control Syst. Technol. 16 (5) (2008) 918–929.

[56] N. Sheikholeslami, D. Shahmirzadi, E. Semsar, C. Lucas, M.J. Yazdanpanah, Applying brain emotional learning algorithm for multivariable control of HVAC systems, J. Intell. Fuzzy Systems 17 (1) (2006) 35–46.
[57] C.P. Underwood, Robust control of HVAC plant I: Modelling, Build. Serv. Eng. Res. Technol. 21 (1) (2000) 53–61.
[58] O. Camacho, C.A. Smith, Sliding mode control: An approach to regulate nonlinear chemical processes, ISA Trans. 39 (2) (2000) 205–218.
[59] E. Bristol, On a new measure of interaction for multivariable process control, IEEE Trans. Automat. Control 11 (1) (1966) 133–134.